E82-10387

AgRISTARS

2.

7. EW-L2-04303
JSC-18243
LEMSCO-17383

NASA-CR-167640

Early Warning and Crop Condition Assessment

A Joint Program for Agriculture and Resources Inventory Surveys Through Aerospace Remote Sensing

6. May 1982

ADVANCED VERY HIGH RESOLUTION RADIOMETER (AVHRR) DATA EVALUATION FOR USE IN MONITORING VEGETATION, VOLUME I - CHANNELS 1 AND 2

3. N. C. Horvath

4. Lockheed Engineering and Management Services Company, Inc.

5. NAS 9-15800

T. I. Gray and D. G. McCrary
National Oceanic and Atmospheric Administration

Lyndon B. Johnson Space Center
Houston, Texas 77058

1. Report No.	2. Government Accession No.	3. Recipient's Catalog No.
EW-L2-04303; JSC-18243		

4. Title and Subtitle	5. Report Date
Advanced Very High Resolution Radiometer (AVHRR) Data Evaluation for Use in Monitoring Vegetation, Volume I - Channels 1 and 2	May 1982
	6. Performing Organization Code

7. Author(s)	8. Performing Organization Report No.
N. C. Horvath, Lockheed-EMSCO T. I. Gray and D. G. McCrary, National Oceanic and Atmospheric Administration	LEMSCO-17383
	10. Work Unit No.
9. Performing Organization Name and Address Lockheed Engineering and Management Services Company, Inc. (Lockheed-EMSCO) 1830 NASA Road 1 Houston, Texas 77258	11. Contract or Grant No. NAS 9-15800
	13. Type of Report and Period Covered Technical Report
12. Sponsoring Agency Name and Address Early Warning/Crop Condition Assessment Project Office USDA, 1050 Bay Area Blvd. Houston, Texas 77058 Technical Monitor: T. I. Gray	14. Sponsoring Agency Code

15. Supplementary Notes

The Agriculture and Resources Inventory Surveys Through Aerospace Remote Sensing is a joint program of the U.S. Department of Agriculture, the National Aeronautics and Space Administration, the National Oceanic and Atmospheric Administration (U.S. Department of Commerce), the Agency for International Development (U.S. Department of State), and the U.S. Department of the Interior.

16. Abstract

Data from the National Oceanic and Atmospheric Administration satellite system (NOAA-6 satellite) have been analyzed to study their nonmeteorological uses. The useful limits of these data were also determined. A file of charts, graphs, and tables was created from the products generated in this study. It was found that the most useful data lie between pixel numbers 400 and 2000 on a given scan line. The analysis of the generated products indicates that the Gray-McCrary Index can discern vegetation and associated daily and seasonal changes. The solar zenith-angle correction used in previous studies was found to be a useful adjustment to the index. The metsat system seems best suited for providing large-area analyses of surface features on a daily basis.

17. Key Words (Suggested by Author(s))	18. Distribution Statement
Gray-McCrary Index meteorological satellite scatterplot transection vegetative index vegetative reflectance	

19. Security Classif. (of this report)	20. Security Classif. (of this page)	21. No. of Pages	22. Price*
Unclassified	Unclassified	94	

*For sale by the National Technical Information Service, Springfield, Virginia 22161

EW-L2-04303
JSC-18243

ADVANCED VERY HIGH RESOLUTION RADIOMETER (AVHRR) DATA EVALUATION FOR USE IN MONITORING VEGETATION

VOLUME I - CHANNELS 1 AND 2

Job Order 72-477

This document describes the meteorological analysis activities of the Early Warning project of the AgRISTARS program.

PREPARED BY

N. C. Horvath
Lockheed Engineering and Management Services Company, Inc.

T. I. Gray and D. G. McCrary
National Oceanic and Atmospheric Administration

APPROVED BY

USDA	Lockheed-EMSCO
G. O. Boatwright, Manager Early Warning/Crop Condition Assessment project, AgRISTARS program	J. K. Oney, Project Manager Early Warning Project Office, Crop Applications Department

LOCKHEED ENGINEERING AND MANAGEMENT SERVICES COMPANY, INC.

Under Contract NAS 9-15800

For

Earth Resources Applications Division

Space and Life Sciences Directorate

NATIONAL AERONAUTICS AND SPACE ADMINISTRATION
LYNDON B. JOHNSON SPACE CENTER
HOUSTON, TEXAS

May 1982

LEMSCO-17383

PREFACE

The Agriculture and Resources Inventory Surveys Through Aerospace Remote Sensing is a multiyear program of research, development, evaluation, and application of aerospace remote sensing for agricultural resources, which began in fiscal year 1980. This program is a cooperative effort of the U.S. Department of Agriculture, the National Aeronautics and Space Administration, the National Oceanic and Atmospheric Administration (U.S. Department of Commerce), the Agency for International Development (U.S. Department of State), and the U.S. Department of the Interior.

CONTENTS

TABLES

FIGURES

ABBREVIATIONS

AVHRR	advanced very high resolution radiometer
CCAD	Crop Condition Assessment Division
CCT	computer-compatible tape
FAS	Foreign Agriculture Service
GAC	global area coverage
GMI	Gray-McCrary Index
GMT	Greenwich mean time
HRPT	high resolution picture transmission
LAC	local area coverage
LACIE	Large Area Crop Inventory Experiment
metsat	meteorological satellite
MSS	multispectral scanner
NOAA	National Oceanic and Atmospheric Administration
pixel	picture element
POES	Polar Orbiting Environmental Satellite
TIROS	Television Infrared Observation Satellite
TIROS-N	Fourteenth of TIROS research series
USDA	U.S. Department of Agriculture

1. INTRODUCTION

Satellites, particularly the Landsat series with its Multispectral Scanner (MSS) system, have made significant contributions to remote sensing. The meteorological satellite (metsat) system of the National Oceanic and Atmospheric Administration (NOAA) has enhanced our knowledge and understanding of the weather. Since the 1960 launching of the first Television Infrared Observation Satellite (TIROS) weather satellite, experimental and operational weather satellites have been launched to test additional instrumentation and new techniques. The resultant technology has provided not only for increased weather forecasting accuracy, but for applications in other areas as well. The advanced very high resolution radiometer (AVHRR) system aboard the TIROS-N[1], for example, can simultaneously observe reflective energy in selected bandwidths of the visible and near-infrared parts of the solar spectrum (similarly to the Landsat MSS system) and can provide data relevant to agriculture.

These new uses of the metsat would complement the higher resolution Landsat data and provide more timely coverage. Landsat revisits the same spot every 18 days. The presence of clouds when the satellite is overhead can be troublesome, impeding the success of data collection. One or more metsat fields of view cover each given area daily. Thus, barring clouds, these images could fill the gaps in Landsat coverage. During the Large Area Crop Inventory Experiment (LACIE), imagery of many selected target areas was acquired by Landsat. These MSS acquisitions were obtained mostly toward the end of the growing season (characterized by clearer, drier weather conditions) and rarely at the important initial stages of growth (personal communication between primary author and D. G. McCrary). At that time, no coincident metsat data were obtained or examined to supplement the Landsat data, because the metsat system was not configured to distinguish vegetation.

[1]TIROS-N is the 14th in the research and development series.

Two recent papers (refs. 1 and 2) describe potential nonmeteorological uses of the TIROS-N series. In these papers, both drought and flood conditions are analyzed successfully using the Gray-McCrary Index (GMI) to detect these extreme situations. Currently, the Crop Condition Assessment Division (CCAD) of the U.S. Department of Agriculture, Foreign Agriculture Service (USDA/FAS) processes an index similar to the GMI in real time; however, the restraints and limits applicable to such indexes are unknown. The primary purpose of this study is to define these limits of acceptability for metsat data.

2. POLAR ORBITING ENVIRONMENTAL SATELLITE CHARACTERISTICS

Since October 1978 satellites of the Polar Orbiting Environmental Satellite (POES)[2] system, designed to operationally monitor global atmospheric phenomena, have carried the AVHRR. Both the AVHRR and the Landsat MSS respond similarly to reflective solar energy. Many previous studies have used the data from Landsat satellites to monitor and assess agricultural activities. This AVHRR system could be used to acquire data sets relevant to the examination of agricultural activities, and such information could be a significant addition to data collected by Landsat.

The characteristics of the above satellite systems have been well documented in previous reports (refs. 2 and 3). An additional report to be issued later will describe the NOAA-7 characteristics. This document is an analysis of the nonmeteorological uses of NOAA-6 satellite data.

Briefly, each satellite system is in a near-polar, Sun-synchronous orbit about 832 to 928 kilometers (520 to 580 miles) above the Earth's surface, orbiting the Earth approximately 14 times daily. Aboard the Landsat, the MSS acquires radiance data in four reflective spectral bands. The POES family carries the NOAA AVHRR system to acquire radiance data in two reflective spectral bands and two or three emittive bands. This system offers the same methods of data transmission as do the Landsat systems - high resolution picture transmission (HRPT), a direct broadcast mode, and local area coverage (LAC), a stored mode for delayed transmission to command data acquisition stations. In addition, the POES provides lower resolution data for global area coverage (GAC) in both modes, although the direct transmission data are computed by a formula different from that used for the stored data.

---

[2]The term POES shall be used to designate the family of satellites based upon the research and development vehicle TIROS-N; the group includes TIROS-N, NOAA-6, and NOAA-7.

The major differences between the Landsat MSS and the NOAA AVHRR systems are in image resolution at nadir, image width, and temporal continuity. At nadir, Landsat images have a resolution of 0.009 square kilometer, while comparable POES images have a resolution of 0.95 square kilometer. Landsat observes the same target every 18 days, assuming the view is unobstructed. However, the POES observes the same targets daily with the same restraints, and it can provide clear views to fill the gaps left by Landsat.

The AVHRR spectral bandwidths of the reflective channels, 1 and 2, were chosen to aid in the detection of snowmelt, an environmental phenomenon relative to hydrological forecasting. The original bandwidths of 1 and 2 on TIROS-N overlapped and were inadequate for the designed purpose. However, a new bandwidth was chosen for channel 1 of the NOAA-6 AVHRR and subsequent AVHRR instruments. This new channel 1 responds to reflected energy in the yellow-red portion (550-700 nm) of the visible spectrum and thus has a minimum response to verdant greens. However, the channel 2 bandwidth responds to the reflected energy in the near-infrared part of the spectrum (700-1100 nm) and acquires high values from vegetation. (See figure 2-1; note both wheat curves.) These characteristic responses from vegetation lead to the comparative use of the near-infrared versus visible data to define vegetative indices. Table 2-1, below, shows some of the available channels for both the AVHRR and the MSS systems.

TABLE 2-1.- COMPARISON OF POES AND LANDSAT CHANNELS AND THEIR ASSOCIATED BANDWIDTHS

[From ref. 4]

POES channel	AVHRR bandwidth	Landsat channel	MSS bandwidth
1	550 to 700 nm	1	500 to 600 nm
		2	600 to 700 nm
2	700 to 1100 nm	3	700 to 800 nm
		4	800 to 1100 nm

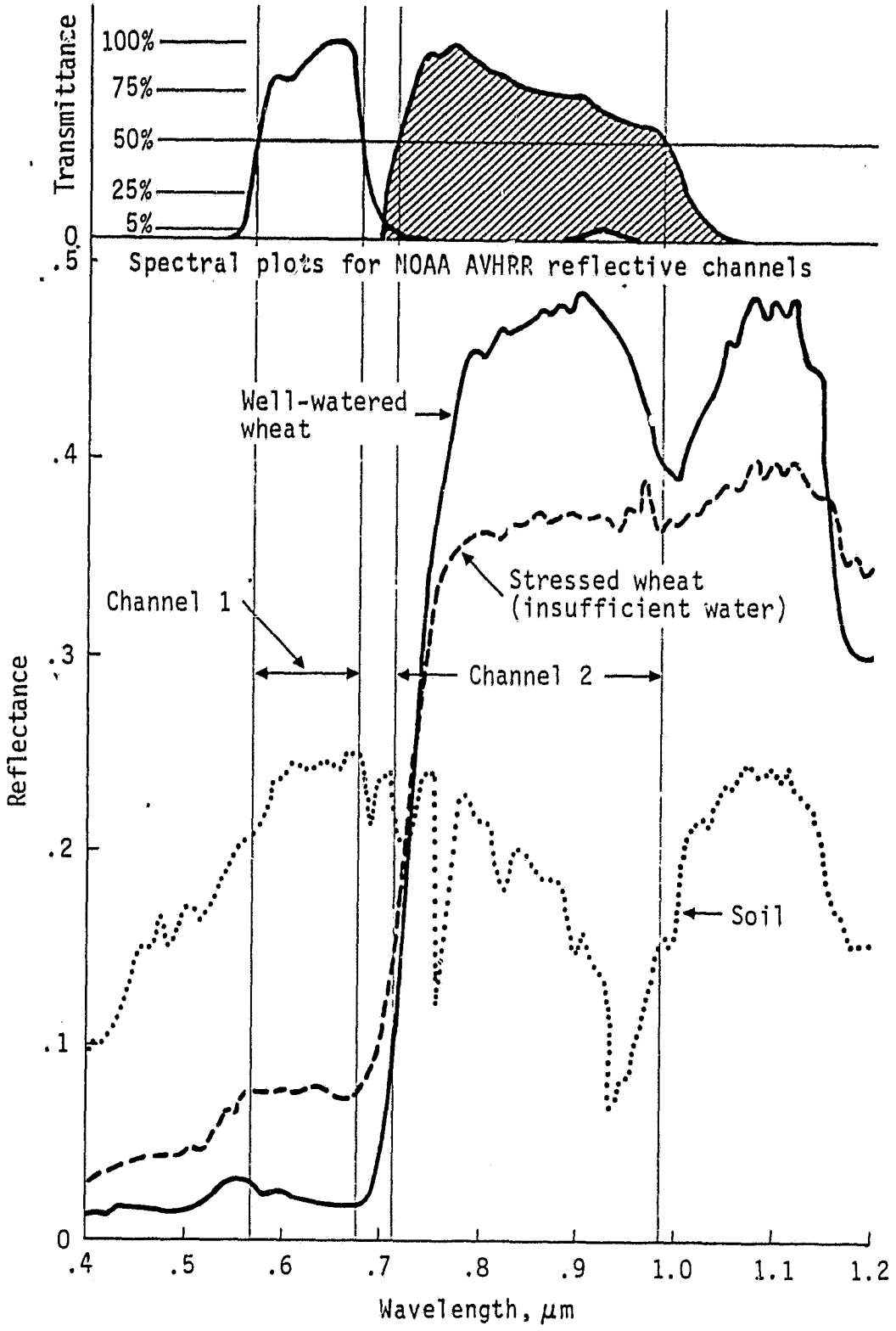

Figure 2-1.- Response of NOAA AVHRR reflective channels (wheat). [From ref. 4]

Two graphs were constructed to display and detail the sensitivity and response of the NOAA AVHRR channels (ref. 1). Figure 2-1 consists of two graphs; one shows the transmittance of the spectral plots for the NOAA AVHRR reflective channels, and the other compares wavelength with reflectance for various surfaces. In the lower graph, the implication of the wheat curves is significant. The curve representing well-watered wheat shows the spectral response for healthy wheat. There are low values in the visible wavelengths and high values in the near-infrared wavelengths, coincident with the limits of channels 1 and 2, respectively. When wheat is stressed, the reflectance in the visible range is enhanced while that in the near-infrared range decreases. Consequently, the difference between these two channels will best show the state of health of the wheat. Also included in this graph is the soil line.

Figure 2-2, in the same format as figure 2-1, shows the spectral responses for asphalt, water, sand, soybeans, and concrete. While the soybean curve shows the vegetative response of low reflectances for wavelengths below 0.7 millimeter and high reflectances for those above, it should be noted that this particular crop was being stressed by an 11.5-percent fungal infestation.

The response of a healthy soybean crop (not plotted in figure 2-2) shows a curve which has an average reflectance that is .37 higher than that of the stressed soybean crop. (See table 2-2).

The water, concrete, and asphalt responses are quite distinctive, enabling one to locate roads, as well as rivers and other bodies of water.

Because coincident Landsat and NOAA-6 data were unavailable, a comparison was not performed. The characteristics of the MSS sensor onboard the Landsat and the AVHRR onboard the POES have both been well documented (ref. 3). The AVHRR collects data for every channel simultaneously. Thus, a picture element (pixel) from any one channel can easily be compared with that from another channel, and there will be a maximum of overlap in the area covered by both pixels. While the overlap of these pixels is not quite perfect, the offset is constant once a satellite is in orbit.

TABLE 2-2.- REFLECTANCE VALUES FOR SOYBEANS IN THE NEAR-INFRARED PART OF THE SPECTRUM

Wavelength, μm	Reflectance, healthy soybeans	Reflectance, soybeans with 11.5% fungal infestation
0.72	0.300	0.202
.75	.578	.229
.78	.579	.252
.81	.695	.275
.84	.697	.319
.87	.722	.338
.90	.759	.347
.93	.749	.362
.96	.733	.386
.99	.702	.417

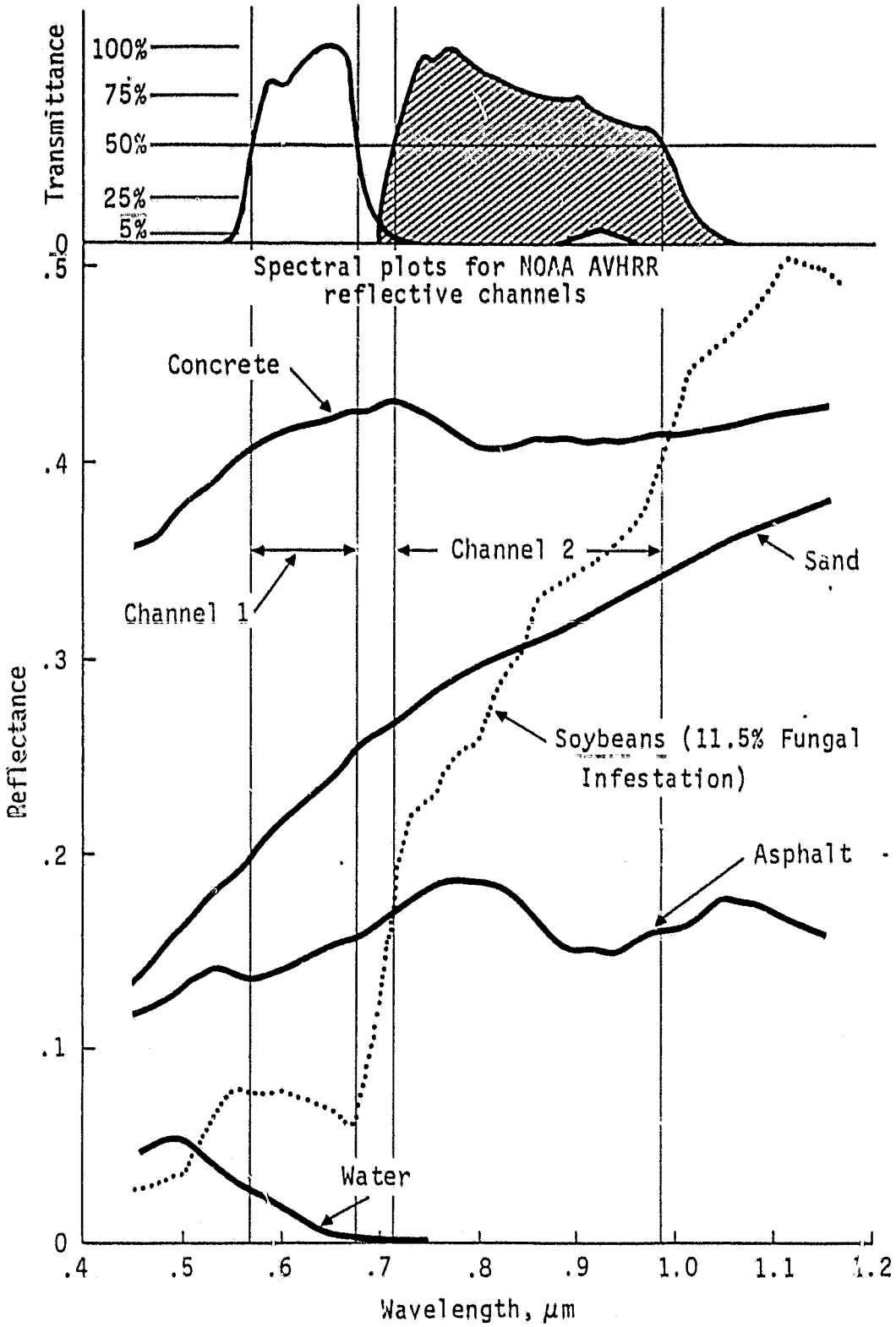

Figure 2-2.- Response of NOAA AVHRR reflective channels (concrete, asphalt, water, sand, and soybeans). [From ref. 4]

3. THE GRAY-McCRARY INDEX

The GMI is defined as the difference in the returns from channels 2 and 1. This index, which emphasizes the variations of healthy vegetation and provides negative responses for clouds and water, is relatively simple and can easily be placed into current operational activities.

Both clouds and water generate higher returns in channel 1 than in channel 2, consequently producing negative GMI values. For both channels, the cloud returns are high and the water returns are low, thus permitting the implementation of an analytical tool, "ramps." These ramps substitute one value for a variable negative result, based upon the characteristics of channel 1. Healthy vegetation has a channel 1 response usually less than 125 raw counts, or 9 percent reflectance. Responses greater than this are indicative of clouds. Thus, the GMI values that include channel 1 returns greater than 9 percent are ramped. We chose to set all cloud values to a ramp of -1.5; all water, snow, and ice values to a ramp of -0.5; and certain indeterminate targets to -1.0. This approach reduces the emphasis of these targets and accentuates the remaining positive quantities for vegetation.

Generally, the values of the GMI vary from -1.5 to 32.0. Healthy vegetation produces values that range from about 8.0 upward. Soils have responses that vary from slightly less than zero to about 4.0 (ref. 5).

The most accurate values of the GMI occur for pure-pixel views. A mixed pixel will contain inputs from many different sources, and thus the GMI value for that pixel will be altered. Pixels over pure vegetation give the highest return. Because any mixed pixel will include soil, water, and cloud responses, its GMI value will automatically be lowered. Figure 3-1, a cross section of a satellite scan line, shows how a mixed pixel is viewed by the AVHRR. A comparison of two pixels, one pure and one mixed, shows that the resultant GMI for the mixed pixel is less than that for the pure pixel. (See figure 3-2.)

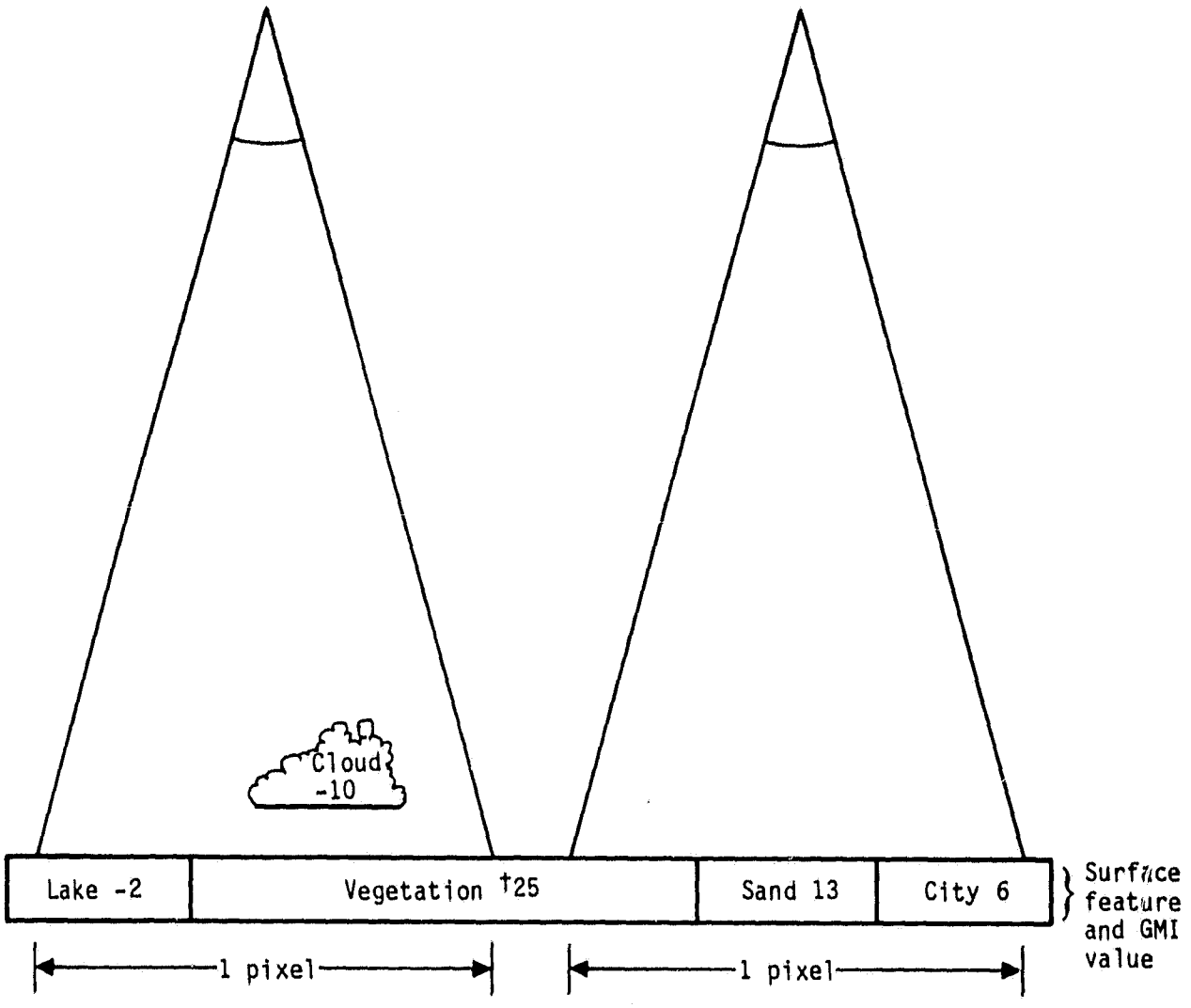

†Vegetation value of 25 could be as low as 18 if plants are under stress.

Figure 3-1.- Cross section of satellite views of mixed pixels.

Pure pixel GMI value

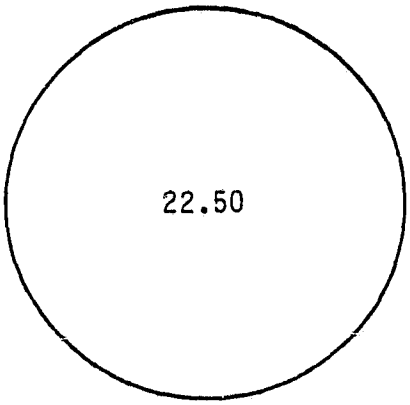

Mixed pixel GMI value

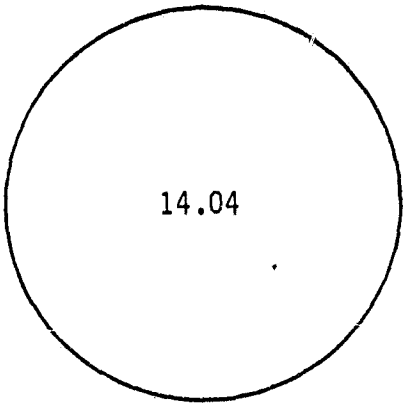

Surface	Value	Surface	GMI value
100% well-watered wheat	24.50 (channel 2)	60% well-watered wheat	13.50
	2.00 (channel 1)	20% soil	.80
		15% clouds	- .23
	22.50 GMI	5% water	- .03
			14.04 GMI

Figure 3-2.- Comparison of synthetic GMI values for pure and mixed pixels.

Scatterplots were generated from the raw data of POES channels 1 and 2 to further determine the GMI values representing soil, water, and green vegetation. These scatterplots show the counts for each channel, the reflectance for each channel, and the subsequent uncorrected GMI values. The scatterplots were each generated using data from an area 40 by 40 kilometers (or 25 by 25 miles) which is represented by one grid square. Five separate grid squares were chosen (see fig. 3-3), each representing an area of consistent surface conditions. Examples of scatterplots appear in appendix A, section 2, and the resultant data from all the scatterplots appear in table 3-1. This table shows the range of GMI values for each plot with respect to date of acquisition and grid square. Descriptions of the surface conditions are included.

TABLE 3-1.- RANGES OF GMI VALUES FOR GIVEN GRID SQUARES

Day	GMI value range					
	Good cropland and Illinois River i,j=235,372	Good cropland i,j=238,374	City of St. Louis i,j=236,375	Forest and Rend Lake i,j=238,377	Ohio and Wabash Rivers and forest i,j=240,378	City of St. Louis i,j=235,375
191	†5 to 7	†7 to 8				
192	†6 to 8	All cloud				
193	†8 to 10	7 to 9				
194	9	8 to 9				
195	†-3 to 7	†6 to 7				
195	†1 to 3, 7 to 9	†6 to 9			All cloud	
196	8 to 10	7 to 8				
197	8 to 10	8 to 9	8 to 9	7 to 9	8 to 9	5 to 9
280	2 to 3	2 to 3				
282	2 to 4	2 to 3				
283	2 to 3	2 to 3		2 to 3	2 to 3	
284	1 to 2	†0 to 2	2			

†Includes contamination by clouds.

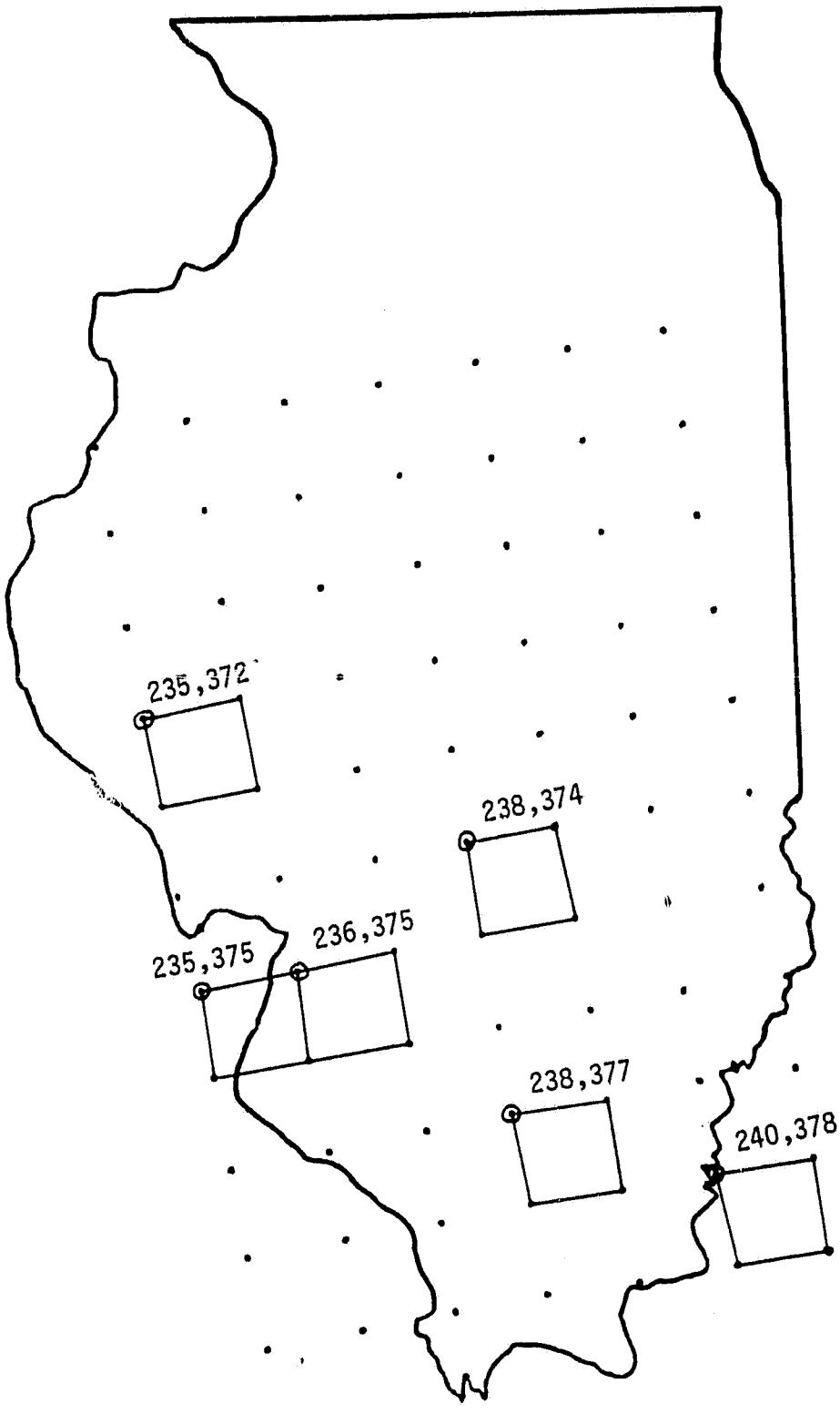

Figure 3-3.- Grid cells (i,j) used for scatterplots.

4. THE TARGET AREA

Illinois lies just south of the Great Lakes, in the Central United States. Two basic land-surface forms are found in this State: (1) smooth plains in the central and northeastern portions and (2) irregular plains over the remaining regions. This land is from 152 to 305 meters (500 to 1000 feet) above sea level. The map in figure 4-1 (ref. 6) shows the potential natural vegetation for the State of Illinois and portrays what the vegetation would look like without the influence of man.

The land use of Illinois is of two types: (1) cropland in the central and northeastern areas and (2) cropland with pasture, woodland, and forest in the southern and western regions, especially along the river valleys. Charts showing the 1979 distribution of major crops in Illinois are given in figure 4-2 (ref. 7). While these charts are not for 1980, previous charts reveal that the specific growing regions have changed very little. It can be seen from these charts that the major portion of corn and soybean production is in the central part of the State.

Figure 4-3, the delineation of the actual area used in this study, shows that while most of the target area lies in Illinois, some portions lie in neighboring states. A grid system was placed over a map of this region to subdivide the acquisition into smaller sections and provide a basis for analysis. The i,j-grid system is a superset of the grid devised by Charney in 1952 (ref. 8) for computer analyses of meteorological data. This superset has the same orientation of that grid system where the i lines are parallel to 80° W. and the j lines to 170° W.

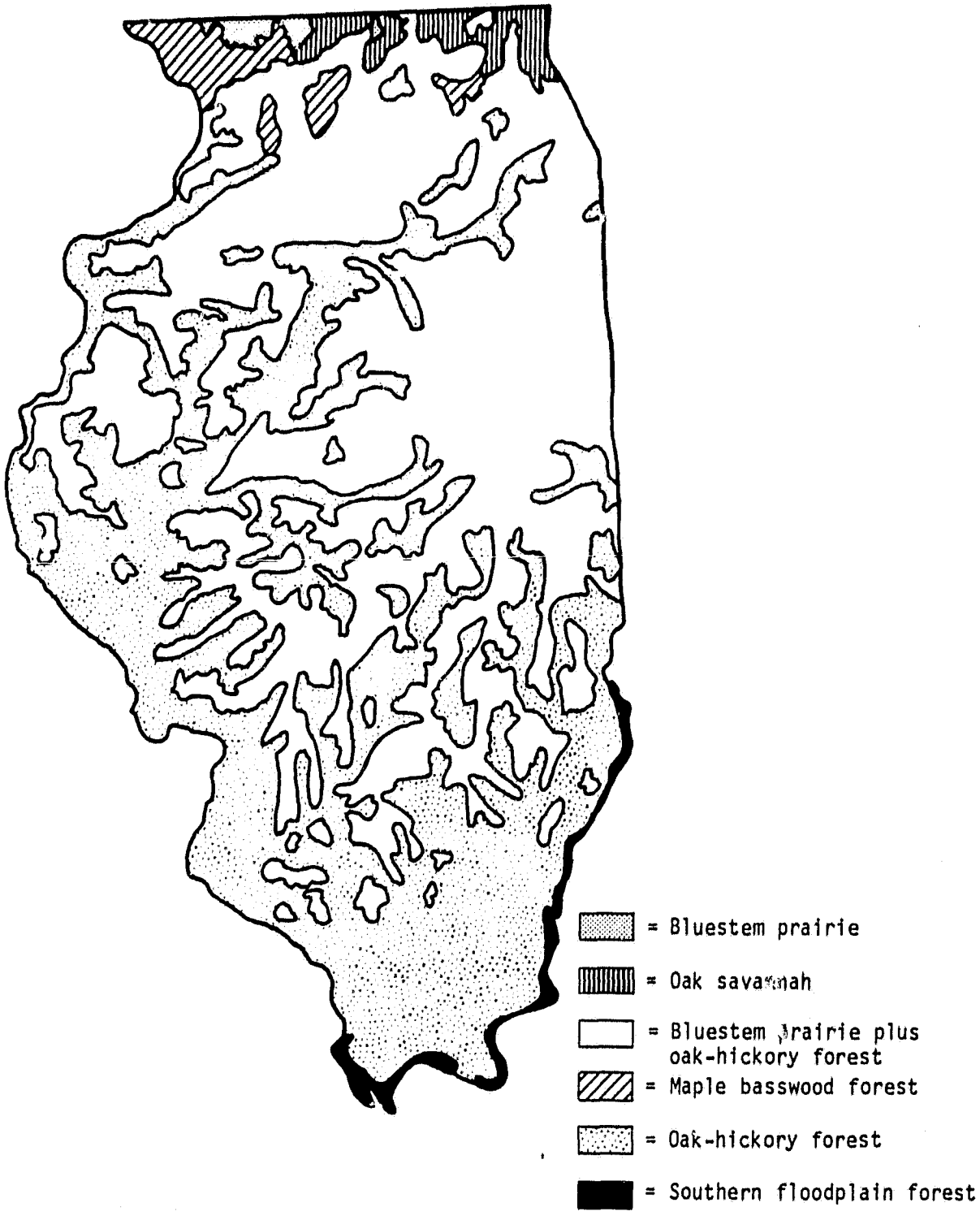

Figure 4-1.- Potential natural vegetation for Illinois (ref. 6).

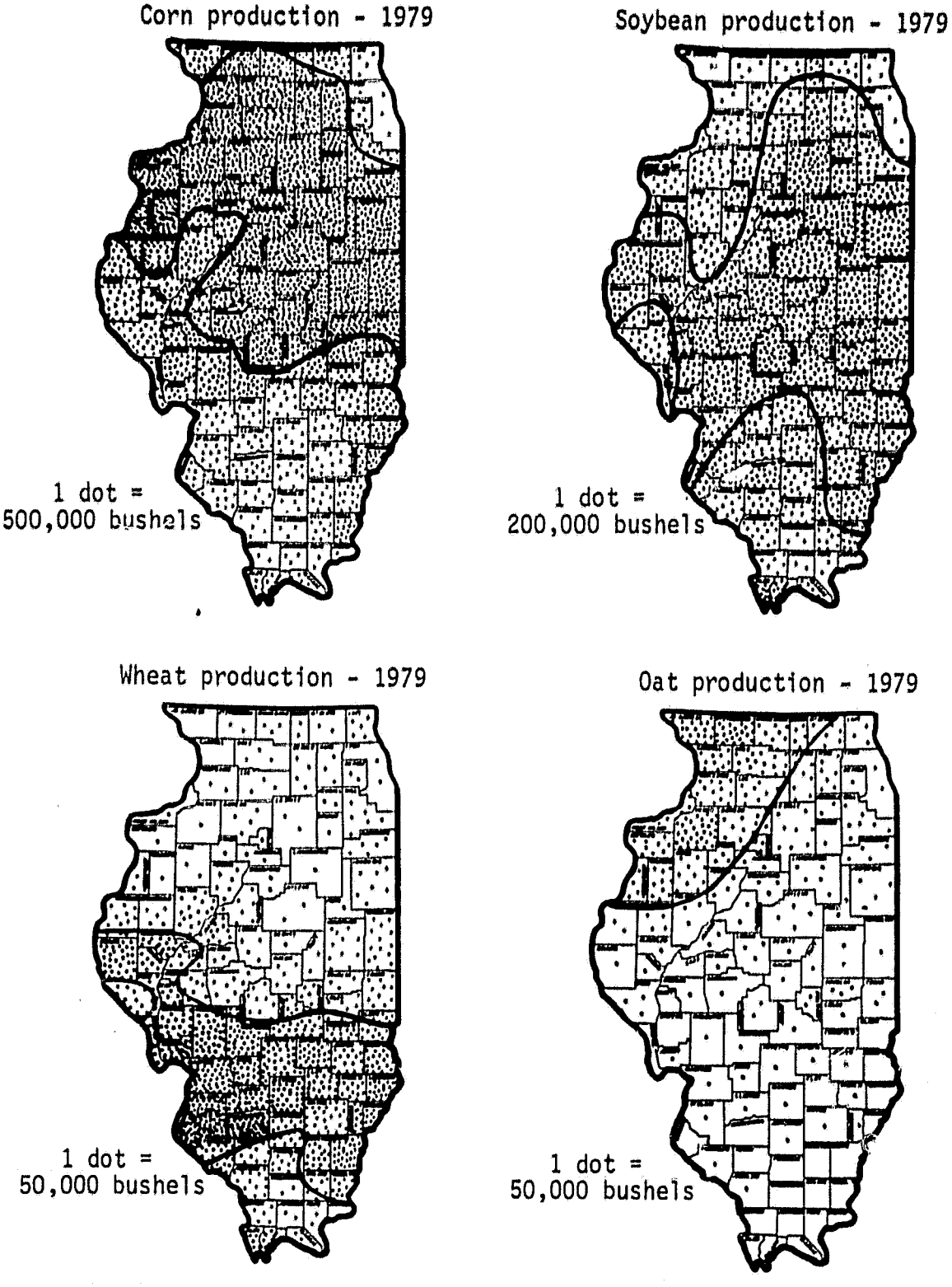

Figure 4-2.- Distribution of major crops (ref. 7).

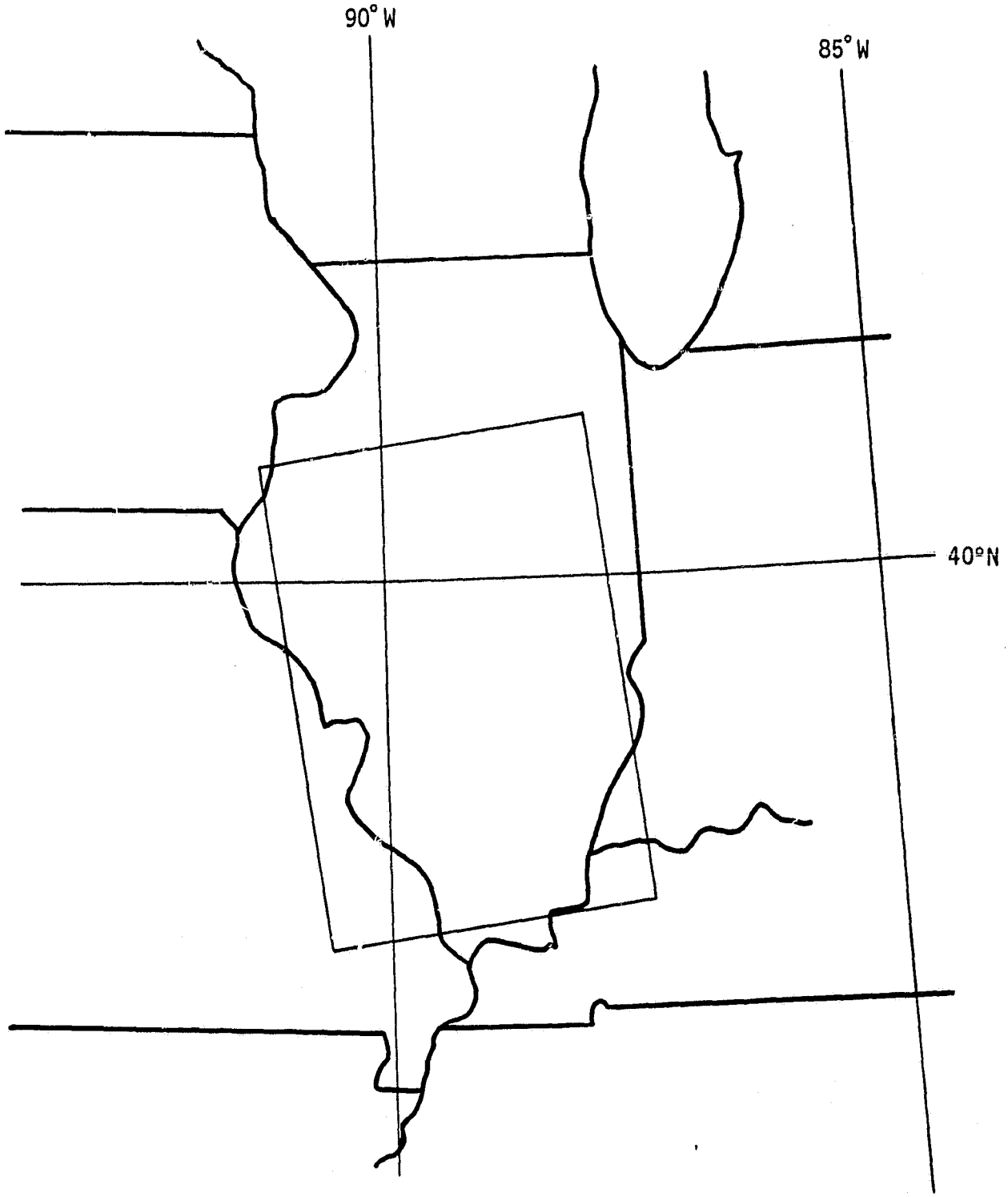

Figure 4-3.- Target area delineated on map of Illinois and surrounding states.

5. EXPERIMENTAL RESULTS

Remote sensing devices can identify and interpret vegetation conditions if the plant signatures are known. If some meteorological phenomenon has hindered the growth of these plants (a stress such as drought, hail, or other severe weather), this condition will change the signature of the plants. Stresses on a plant, i.e., those conditions that prevent the plant from reaching its full growth potential, need to be monitored. Figure 2-1 shows the results of stress on wheat, and the change in signature from the healthy condition is readily apparent. For this reason, a weather analysis was performed. Figure 2-2 shows a stressed soybean crop, this time the cause being an 11.5-percent fungus infestation. Thus, nonmeteorological stresses can also create detectable GMI signatures. If weather and health conditions are less than optimum, plants have a reduced greenness. Certain plant stages, such as senescence, will produce a "brown-up" condition, or drop in values of greenness. Results of this crop growth study (the forms of the curves, etc.) were expected to be similar to those of the 1979 study by Thompson and Wehmanen (ref. 9).

5.1 WEATHER DATA ANALYSIS

Three major sources, all U.S. Government publications, were used to examine and analyze weather conditions for both the July and October 1980 time periods. These were the "Daily Weather Maps, Weekly Series" (ref. 10), the "Weekly Weather and Crop Bulletin" (ref. 11), and "Climatological Data" (ref. 12). The "Daily Weather Maps, Weekly Series" and the "Weekly Weather and Crop Bulletin" were used to determine the general weather patterns and conditions for the test site. The information from "Climatological Data" was used to make a precipitation analysis, which appears in appendix A, section 4.

Weather conditions for July 9 through 15, 1980

Temperatures were 6° to 14° above normal in the area because of a high pressure cell aloft over the U.S. central Great Plains. There was shower activity

over the State of Illinois, but significant rain fell only in the first 3 days of the acquisition period. A weak frontal system was located across central Illinois at the beginning of the time period, but by July 13 it had moved southward. Onshore flow from Lake Michigan, occurring July 9, 10, and 13, explains some of the cloudiness present then. Thus, the low GMI values and unusually high channel 1 values are probably due to subresolution cloudiness.

Weather conditions for October 6 through 10, 1980

Temperatures were 1° to 8° below normal, and no significant precipitation fell during the acquisition period. There were two frontal passages; basically, however, skies over the target area remained clear. There was some onshore flow on October 9, but no resolvable cloudiness was observed.

5.2 AGRICULTURAL DATA ANALYSIS

The "Weekly Weather and Crop Bulletin" provided the main source of information about agricultural conditions within Illinois; these data are reproduced in their entirety in table 5-1. The spring of 1979, used for comparison in the reports below, was very wet; consequently, crops either were not planted, were planted late, or (for those already in the ground) were late in maturing.

The maximum values of the GMI are expected to be found for healthy crops. When these crops are harvested or stressed, their GMI values will be lower. Also, the GMI values will be reduced for a healthy crop if a large portion of the ground is visible, such as in the beginning growth stages. Comments on expected GMI values are inserted into the following crop reports, based on the State of Illinois, for the dates given.

5.3 SATELLITE DATA ANALYSIS

The data used in this study were collected by the NOAA-6 satellite and recorded at Wallops Island, Virginia, from real-time transmission. These HRPT data are identical in content to the LAC data, which are scheduled and collected by the NOAA-6 satellite and then stored for later transmission. Calculations of GMI values, attendant corrections, and analyses were performed

TABLE 5-1.- WEATHER AND CROP CONDITIONS FOR TARGET AREA, 1980 DATA

[From ref. 11]

Condition	July 7-13	July 14-20	October 6-12
Temperature	6° to 13° F above normal	7° to 14° F above normal	1° to 6° F below normal
Precipitation	0.30 to 1.00 in. in northern two-thirds, none south	3.0 in. to none	Little or none
Soil moisture	Adequate to short	Short	46% short, 53% adequate, 1% surplus
Corn	23% E, 65% G, 12% F Average height 66 in. [55 in. 1979, 62 in. ave.] Most advanced 80 in. [70 in. 1979, 78 in. ave.] 43% silked, [14% 1979, 37% ave.]	G to F 84% silked [40% 1979, 63% ave.] 15% dough [2% 1979, 11% ave.]	61% harvested (low GMI value) [20% 1979, 27% ave.]
Soybeans	5% E, 75% G (high GMI value), 20% F 53% blooming [35% 1979, 40% ave.] 14% setting pods [5% 1979, 12% ave.]	G to F. 76% blooming, [53% 1979, 24% ave.]	81% harvested (low GMI value) [73% 1979, 67% ave.]
Winter wheat	90% harvested (low GMI value) [86% 1979, 89% ave.]	98% harvested (low GMI value) [98% 1979, 97% ave.]	Acreage 60% seeded (low GMI value) [50% 1979, 51% ave.] 15% emerged [15% 1979]
Oats	5% E, 64% G, 31% F 70% turning yellow (low GMI value) [72% 1979, 79% ave.] 25% ripe [27% 1979, 44% ave.] 10% harvested [2% 1979, 19% ave.]	98% turning yellow (low GMI value) [90% 1979, 93% ave.] 55% ripe [39% 1979, 65% ave.] 30% harvested [25% 1979, 43% ave.]	
Alfalfa	12% E, 73% G (high GMI value), 15% F 55% second crop cut [69% 1979, 56% ave.]		
Barley	50% harvested (low GMI value)	75% harvested (low GMI values)	
Pasture	4% E, 46% G, 46% F, 4% P	22% G, 56% F, 22% P	3% E, 43% G, 51% F, 3% P
Sorghum			60% harvested (low GMI value)
Plowing			1981 corn and soybean acreage 20% complete [8% 1979, 8% ave.]
Fieldwork	5.5 days suitable	6.5 days suitable	7.0 days suitable

Crop condition percentages: E = Excellent, G = Good, F = Fair, P = Poor.

by both machine and analyst. Lists of computer programs and data tapes used appear in appendixes B and C, respectively.

The GMI value was calculated for each pixel over the study area. These values were averaged for each i,j-grid square and then corrected; the resultant number was then placed at the center point of the grid square. A solar zenith-angle correction was applied to the averaged GMI values to simulate a condition of the same sun angle, regardless of the actual sun angle. The equation for the corrected GMI value is:

$$GMI^* = GMI(\sec^2 z)(\cos 39°)$$

where GMI* is the corrected GMI value and z is the solar zenith angle for the given pixel location. The value of 39° was chosen to adjust the data to the nominal solar zenith angle of Landsat scenes.

The data fields of corrected GMI values were then analyzed using meteorological techniques; the results of the analyses appear in section 1 of appendix A. Concomitant with these products were charts of solar zenith angle and pixel number (appendix D). Thus, with these two sets of charts, one can see how the GMI value varies with pixel number, as well as with the surface condition.

Two graphs were made to clarify the satellite look-angle geometry and pixel distortion. The look angle of the AVHRR is approximately 55° on either side of nadir and contains 2048 pixels for each scan. The graph in figure 5-1 shows the width of each Illinois acquisition compared to the entire look angle, plus the ranges of the GMI values. Figure 5-2 (ref. 12), a graph of pixel length versus pixel number, shows how pixel size increases outward from nadir.

Cross sections, or transections, of each data set were produced for specified lines on selected days. These transections, actually plots of the maximum GMI values for each 50 pixels along a scan line, cut across the central and eastern United States, showing the change in the GMI values from west to east. Areas containing water and areas with cloud cover were easily discerned

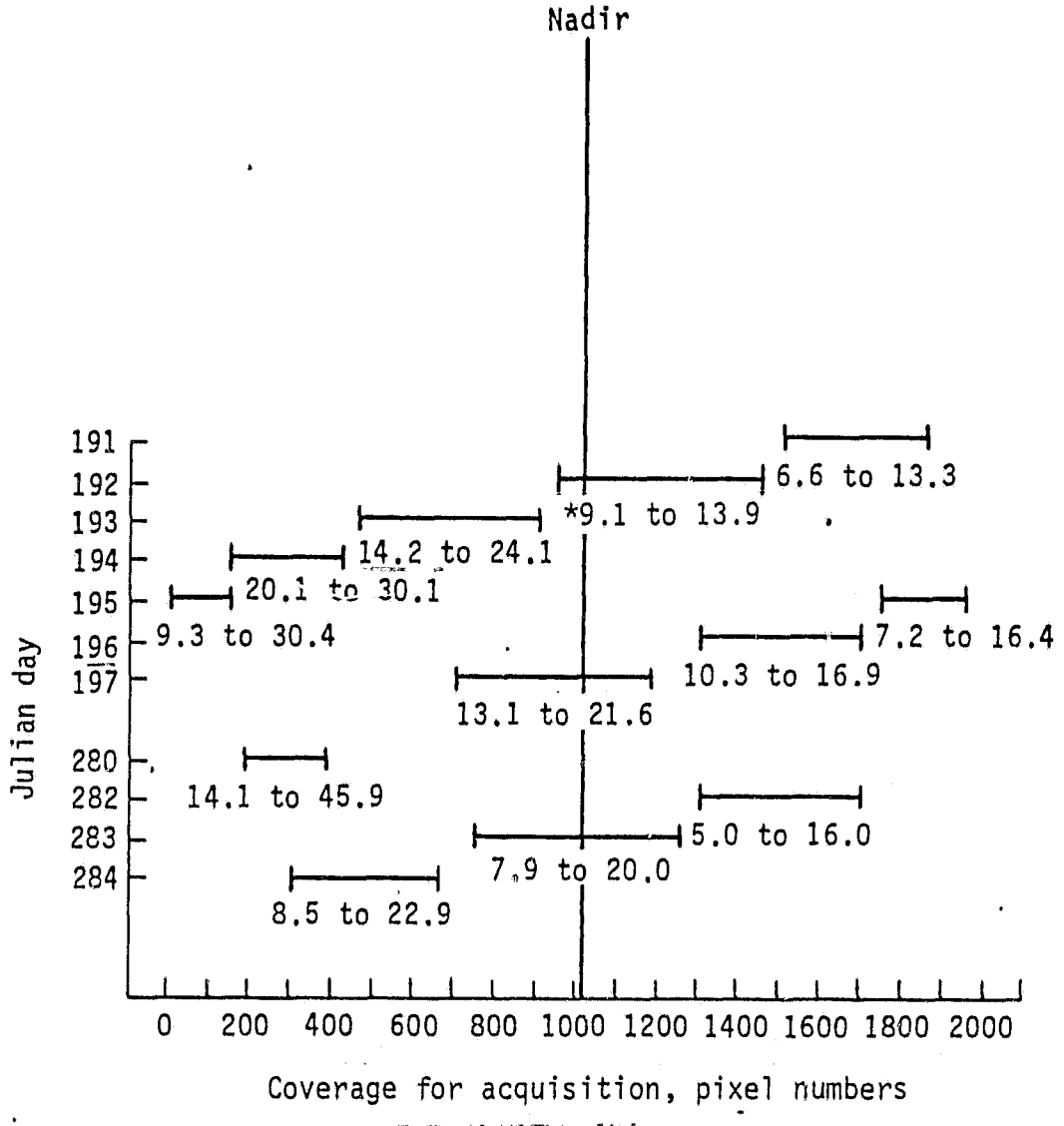

*Range of GMI values for acquisition.

Figure 5-1.- Width and relation to nadir of each acquisition on a scan line.

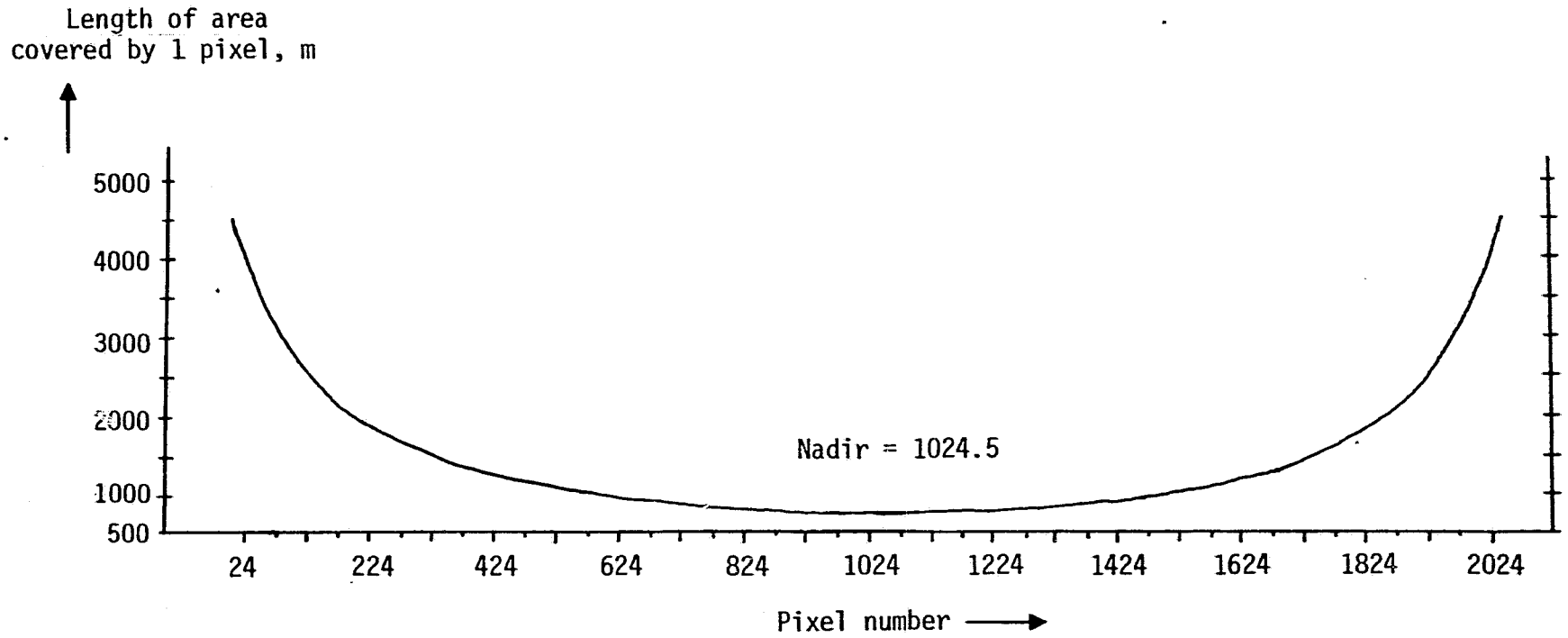

Figure 5-2.- Plot of pixel length away from nadir (ref. 12).

because of the ramping technique. Each transection was checked and fitted geographically by correlating data with locations of appropriate lakes, rivers, and shorelines. The scan lines were drawn on a map of the United States so that a common data point from each corresponded to the same location in southern Illinois, the Carlyle Reservoir. This made line-to-line data comparisons possible because of near geographical coincidence. The raw values for channels 1 and 2 data were also displayed in a similar manner. Both of these analyses appear in appendix A, section 3.

An additional contour analysis was performed on the Illinois GMI* data fields. The maximum GMI* values for the given weekly periods in July and October were plotted and analyzed; these values appear in figure 5-3.

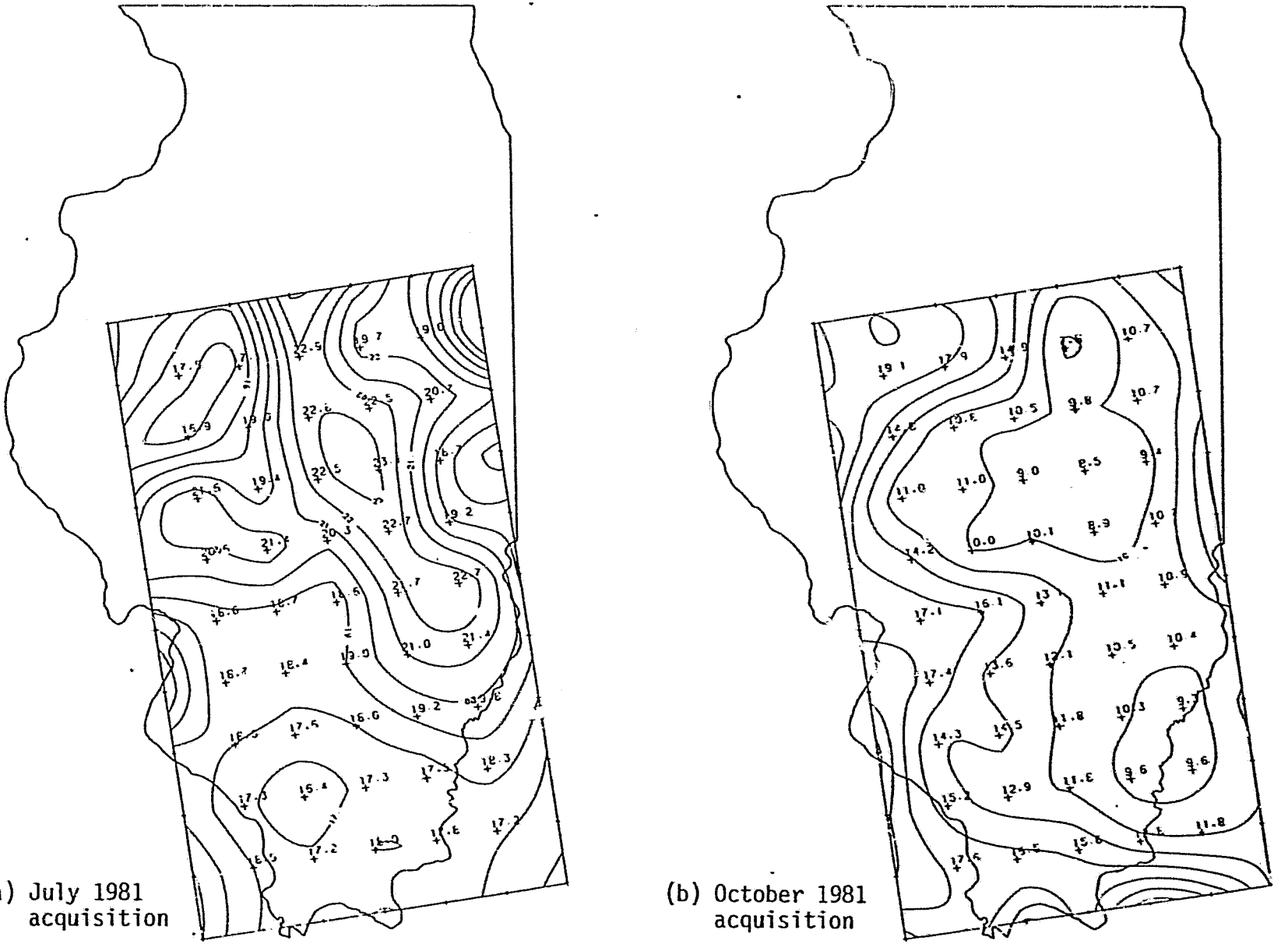

(a) July 1981 acquisition

(b) October 1981 acquisition

Figure 5-3.- Maximum GMI values.

6. ANALYSIS AND INTERPRETATION OF RESULTS

In this section the previously mentioned charts and graphs are examined, and their interpretations are discussed. In a study of this type, all available relevant data should be examined. The use of multiple methods of analysis is far more advantageous than dependence upon one particular system or procedure.

6.1 SCATTERPLOTS

A total of 33 scatterplots was produced to determine the AVHRR responses to various surface conditions. Ranges of GMI values as they relate to specific surface features have been classified in previous studies (refs. 1 and 2). This effort, though similar, also includes a look at temporal changes in the GMI values. Table 3-1, which shows the range of GMI values for given grid squares, includes the corresponding dates and descriptions of the surface conditions. The July ranges are all greater than those of October. In July, the natural vegetation and crops (corn and soybeans) appear green and thus have GMI values in the 6 to 10 range. The October ranges (2 to 3) seem to depict harvested fields (bare soil) and the autumn coloring of the forest. The areas surveyed in October might include bare trees, thus making the ground visible to the sensor.

Many lakes and most rivers are not easily discernible in scatterplots, since such bodies of water are usually less than 1.5 kilometers in width (or slightly wider than the satellite's nadir resolution) and do not present a pure-pixel return. Consequently, water usually appears only in mixed pixels and is often difficult to see on the imagery for this period. Also, because the entire target area (see fig. 4-3) was stressed from drought conditions during July and water levels were low, lakes, reservoirs, and rivers likely were narrower than usual, thus making them more difficult to discern.

The wide range of GMI values for the St. Louis area seems to indicate that the city includes large areas of trees and parkland. These tree-covered areas would explain the resemblance of some city plots to those of forest and

cropland and would account for the change in GMI range for data gathered in autumn.

Nine of the scatterplots show some degree of cloud contamination. Most of these plots are from July periods, when there was some frontal activity in Illinois. While it is easy to gauge the effect of large cloud fields, it is difficult to assess the contamination due to subresolution cloudiness. As shown earlier, clouds contribute negatively to the mean GMI value. These clouds will contaminate otherwise high-value pixels, producing mixed pixels with lower returns. Cloud contamination can also mask ground conditions, or give a completely false interpretation to actual surface conditions. Thus, healthy, growing vegetation could appear on the imagery like plants in senescence when subresolution clouds cover the area.

6.2 GMI* DATA ANALYSIS

The charts of the GMI* values were produced to examine spatial and temporal changes in the index over the target area. One chart was made for each day in both the July and October periods. Cloud-covered areas were determined and analyzed using standard nephanalysis procedures. Transections across the target area were navigated or positioned using these charts.

A persistent minimum feature was found in the data collected for St. Louis during the July period. This seems to be reasonable, because a city consists of concrete, asphalt, and other surfaces that offer lower returns than does vegetation.

Temporal changes in the GMI* were observed after rainfall. The precipitation map of July 10 coupled with the GMI* analyses for July 11 and 12 produced the most graphic example. During the 24-hour period after the rain fell, the GMI* values were low for the specific area covered by precipitation (northwest section of the target area). In the following 24 hours an increase in the GMI* values was observed for the same area. This change can be explained by considering surface conditions during this time period: For the 24-hour period immediately after the rain fell, the ground and plants probably were

still wet, thus producing low-return signatures and subsequent low GMI* values. Then, in the next 24 hours, when surface conditions had become drier, the plants appeared greener, either having benefited from the additional moisture, or having become cleaner because the rain washed any dust and dirt off the plants.

6.3 SOLAR ZENITH-ANGLE CHARTS

The solar zenith-angle charts (appendix D) and the comparison of satellite zenith angles and nadir angles with pixel numbers (appendix E) show how solar zenith angle and pixel numbers change across the target area on a specific day. It has been found that views with low pixel numbers (below 400) tend to have excessively high GMI* values. This is due to the solar zenith-angle correction, sec z, which increases rapidly above 70°. Illumination of the target does not change above 70° according to the sec z correction. This problem was further examined using cross sections of the target area, a method which offered better results.

6.4 TRANSECTION ANALYSES

Both the corrected and uncorrected GMI values are shown in appendix A, section 3. While they have almost identical characteristics, the corrected GMI curve has a sharper slope than does the uncorrected GMI curve. The west-to-east slope of these curves (low pixel numbers to the west) might be explained by land forms and vegetative cover. The western ends of these cross sections lie in the crop-growing area of the Central United States. A survey of these regions suggests high GMI values, but not necessarily as high as shown (because of the effect of the solar zenith-angle correction). East of this region, the land becomes more forest covered, especially in the Appalachian Mountains. Finally, at the east coast, along with the large urban areas, water signatures predominate because of the bays, the marshes, and the ocean itself. Another factor to consider is the solar elevation angle when these data were collected. At 0700 (in the morning) the Sun tends to be low in the east; thus, the eastern half of the scan will be sensing forward-scattered radiation, and the western half of the scan will be sensing backscattered radiation.

Additionally, transections were made of the actual raw-pixel values from channels 1 and 2. (See appendix A, section 3.) A value of 125 for channel 1, which was considered the lower cutoff for clouds, is seen in each graph as a dark horizontal line. All of these raw-pixel-value curves slope upward at the ends, while the central portions are rather flat. The end effects are due to increased forward scattering on the eastern part of the scan line and increased back scattering on the western part of the scan line and are the result of the Sun-Earth-satellite geometry. Thus, while pixel size does increase away from nadir, the predominant end effects are due to preferential scattering of the incident radiation. Because of this systematic end distortion, the flat, central part of each curve probably offers the most reliable data. However, when the GMI is calculated (channel 2 minus channel 1) for a transection, the difference filters out the curve effect.

6.5 RESOLUTION DETERIORATION CONSIDERATIONS

Graphs were drawn to display pixel deterioration away from nadir and to determine the usable portion of the scan line. Figure 5-1 shows that the largest range of values appears on the low-pixel-number, or western, end of the scan line. The collection of data begins in the west, or away from the Sun, and the data are collected toward the Sun. Because of the early morning acquisition time, the western end of the scan line is contaminated by shadows and the eastern part of the scan line is contaminated by Sun glint. Also included here is the portion of the scan line covered by the Illinois target area. The location of the Illinois area on the scan line will determine the number of pixels included in said area. On day 195 the imagery of Illinois had 145 pixels, whereas on day 197 the same section was covered by 480 pixels. This difference is attributed to the way in which pixels change in size away from nadir, as shown in figure 5-2. At the edge of a scan line, the pixels are longer, thus covering more area individually.

These two graphs, in conjunction with the daily GMI* charts, were used to determine what parts of the scan line should be eliminated. If the central 1200 pixels are used and the outer portions are discarded (400 pixels on either end), the data remaining will be of good quality, thus eliminating

extreme GMI* values and minimizing errors which are due to pixel size. This is a symmetrical correction around the nadir point. However, as seen in figure 5-1, the GMI* values on the high-pixel-number, or up-Sun, end of the scan line seem to have acceptable ranges. Therefore, to include the maximum amount of usable data, only the 400 pixels on the low-pixel-number, or down-Sun, end should be discarded. Further investigation is needed; data taken at noon and afternoon, local time, should be examined and compared with the data used in this study. Since data acquired at local noontime would not reflect serious Sun-angle problems, this time would be best for data collection.

6.6 DATA AND INDEX CORRECTIONS

Calculations of the GMI values were performed both with and without a secant solar zenith-angle correction. In all cases the shapes of contours and patterns of lines were very similar. For example, the GMI transections are different only because the corrected line is pivoted from the uncorrected line. Thus, it could be said that the correction is unnecessary. This assumption is satisfactory for day-to-day comparisons over a 3- to 4-day period, and a great deal of information without the correction does exist. The solar zenith angle changes slowly, and its added secant correction could be deleted. However, for weekly or monthly comparisons of GMI values, the secant correction is necessary. This correction will give all the data the same sun angle and make the comparisons, especially the monthly ones, much more valid.

The radiation impinging on the AVHRR is reflected radiation from the surface of the Earth and is thus subject to absorption and scattering by the atmosphere. This attenuation will vary with the weather and with the composition and state of the atmosphere. This phase of the problem, variation due to atmospheric conditions, was not considered in this study. While all the index values used in this study are relative rather than absolute, an understanding of atmospheric attenuation would make spatial and temporal comparisons of the GMI values more accurate and perhaps would eliminate problems caused by subresolution cloudiness and haze.

6.7 CHARTS OF WEEKLY GMI* MAXIMUMS

Probably the best way to utilize this index is through the use of the analyzed fields of weekly GMI* maximums. GMI* maximums were selected to minimize atmospheric attenuation. Since clouds and other obscuring phenomena lower the GMI* value, high values of this index will coincide with relatively clear days. Figure 5-3 shows the GMI* maximums for the July and October acquisitions. In these particular charts, data from days which appeared on the low-pixel-number end of the scan were eliminated. Other charts, which were constructed using acquisitions from all days and also noncorrected data, were not as satisfactory. The resulting patterns on these GMI* value charts were then compared with the chart of the distribution of major crops (fig. 4-2) and with the agricultural analysis.

In July the central maximum area on the chart of GMI* values corresponds with the areas normally planted in corn and soybeans. The southern minimum areas correspond to the wheat-growing regions. The axis of the minimum area in the northwestern part of Illinois lies along the valley of the Illinois River, and a minimum value also appears for an area centered in St. Louis.

When the agricultural data analysis was examined, both the corn and soybeans were found to be reasonably healthy (high GMI* values); the wheat was almost completely harvested (low GMI* values); and the oats were turning yellow (low GMI* values).

For October, the central minimum area corresponds with the corn and soybean area, which at this time was more than 50 percent harvested (low GMI* values). The wheat areas were undergoing planting or plowing and consequently had a similar response (low GMI* values) to that for July. Wheat is grown on a smaller scale in Illinois than is corn or soybeans. Consequently, the low GMI* values over the wheat growing region might not reflect the health of that specific crop. However, this area did have some of the highest temperatures and the least amount of rainfall during the July and October acquisitions. Consequently, the low GMI* values there could indicate the amount of stress on all the vegetation.

These comparisons indicate that cultivated vegetation can be observed with the NOAA AVHRR. While the GMI produces broad-area estimates and can make only a gross estimate of vegetative conditions, it could be a useful tool and adjunct to current operational systems.

7. SUMMARY OF RESULTS

In this study, the feasibility and practicality of nonmeteorological uses of data collected by the NOAA-6 satellite have been examined, using the GMI as the basic tool for examination. Associated tapes, charts, graphs, and tables were prepared in conjunction with the study. The analysis of these products indicates that this index can discern vegetation. Daily or seasonal index changes appear to be related to stress and/or growth variations. Suggested usable limits of the data were determined. The solar zenith-angle correction that has been used in previous studies was examined and found to be a useful adjustment to the index. The metsat system seems best suited for providing large-area analyses of surface features on a daily basis. These products can then be combined and operated upon to produce appropriate weekly analyses.

Additional studies need to be undertaken to determine:

- The time changes of this index for "normal" crop calendars
- The capabilities of the AVHRR in detecting the onset of disease or other stress conditions
- The content and value of information from the other AVHRR channels
- The information gained from comparing data from the reflective channels and the GMI with data from the other AVHRR channels

8. REFERENCES

1. Gray, T. I., Jr.; and McCrary, D. G.: Meteorological Satellite Data - A Tool to Describe the Health of the World's Agriculture. AgRISTARS Report EW-N1-04042, JSC-17112, 1981, 7 pp.

2. Helfert, M. R.; McCrary, D. G.; and Gray, T. I.: Utilization of Meteorological Satellite Imagery for World-Wide Environmental Monitoring of the Lower Mississippi River Flood of 1979 - Case 1. AgRISTARS Report EW-N1-04104, JSC-17144, 1981, 26 pp.

3. McCrary, D. G.; Gray, T. I.; and Armstrong, T. E.: Characteristics of TIROS, GOES, DMSP and LANDSAT Systems. AgRISTARS Report EW-N1-04075, JSC-17131, LEMSCO-16504, 1981, 17 pp.

4. Gray, T. I., Jr.; and McCrary, D. G.: The Environmental Vegetation Index, a Tool Potentially Useful for Arid Land Management. AgRISTARS Report EW-N1-04076, JSC-17132, 1981, 3 pp.

5. Gray, T. I., Jr.; and McCrary, D. G.: An Application of Advanced Very High Resolution Radiometer Data to Monitor the World's Agriculture. (In press).

6. Küchler, A. W.: Potential Natural Vegetation of the Conterminous United States. American Geographical Society (New York), 1975.

7. Illinois Agricultural Statistics, Annual Summary, 1980. Illinois Cooperative Crop Reporting Service (Springfield), 1980.

8. Charney, J. G.; and Phillips, N. A.: Numerical Integration of the Quasi-Geostrophic Equations for Barotropic and Simple Baroclinic Flaws. Journal of Meteorology, vol. 10, no. 2, April 1953, pp. 71-99.

9. Thompson, D. R.; and Wehmanen, O. A.: Using Landsat Digital Data to Detect Moisture Stress. Photogrammetric Engineering and Remote Sensing, vol. 45, no. 2, Feb. 1979, pp. 201-207.

10. Daily Weather Maps, Weekly Series. U.S. Department of Commerce, NOAA, Environmental Data and Information Service. July 7-13, 1980; July 14-20, 1980; Oct. 6-12, 1980.

11. Weekly Weather and Crop Bulletin. U.S. Department of Commerce, NOAA, Environmental Data and Information Service; USDA Economics, Statistics and Cooperative Service, vol. 67, no. 29, July 15, 1980; vol. 67, no. 30, July 22, 1980; vol. 67, no. 42, Oct. 15, 1980.

APPENDIX A

ANALYZED CHARTS AND GRAPHS

APPENDIX A

ANALYZED CHARTS AND GRAPHS

The charts and graphs contained in this appendix were prepared as a part of the study undertaken in response to task action document 63-2457-2477-03.

Sections 1 through 4 display results of various analyses performed on the available data. The contents of the sections are as follows:

- A.1 GMI* data analyses
- A.2 Scatterplots
- A.3 Transections
- A.4 Precipitation analysis

A.1 GMI* DATA ANALYSES

The figures in this appendix show the results of analyses of AVHRR data. Numbers shown on the maps represent corrected GMI values, and shaded areas indicate cloud cover. Beside each map is indicated the Julian day, the date, and the Greenwich mean time (GMT) for the acquisition.

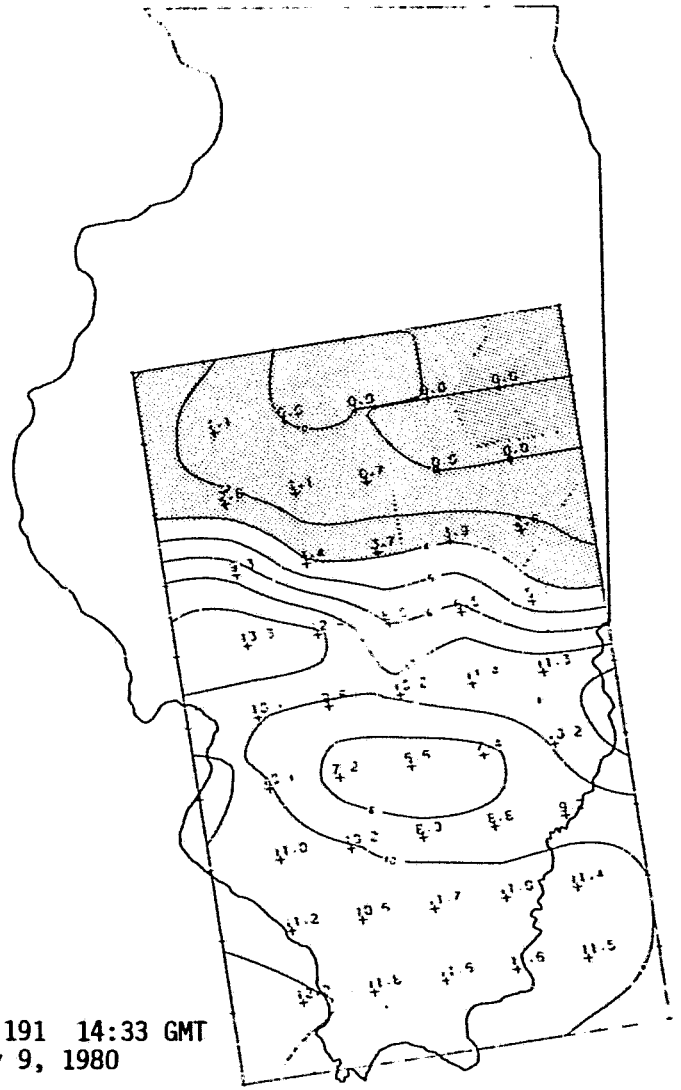

Day 191 14:33 GMT
July 9, 1980

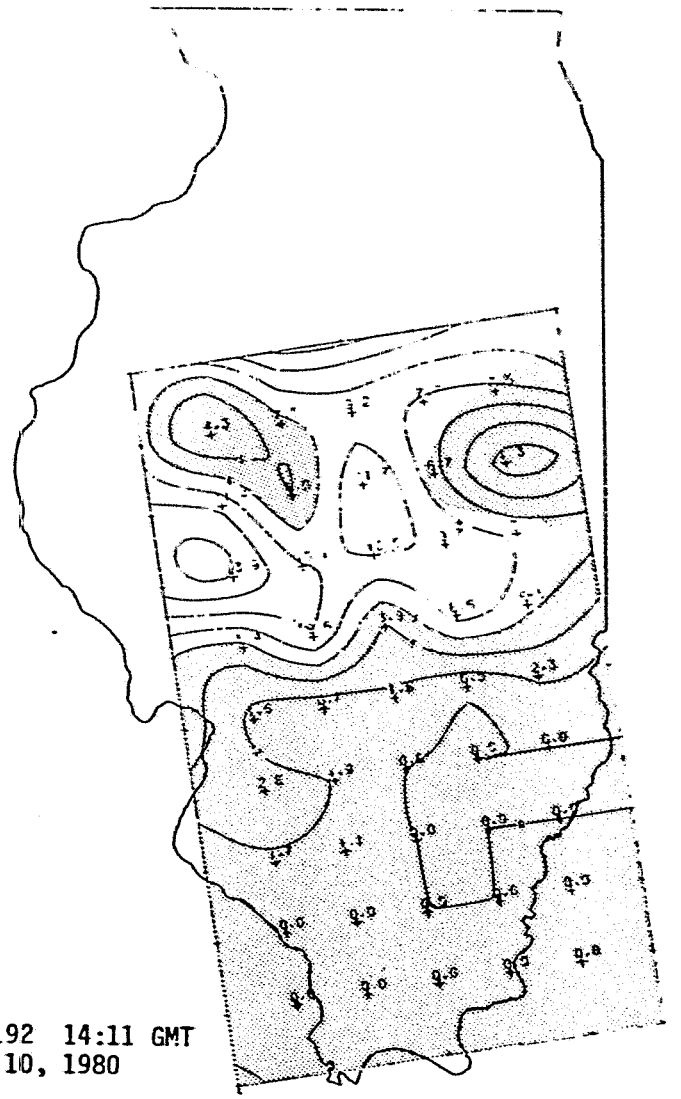

Day 192 14:11 GMT
July 10, 1980

Figure A.1-1.- GMI* Analysis.

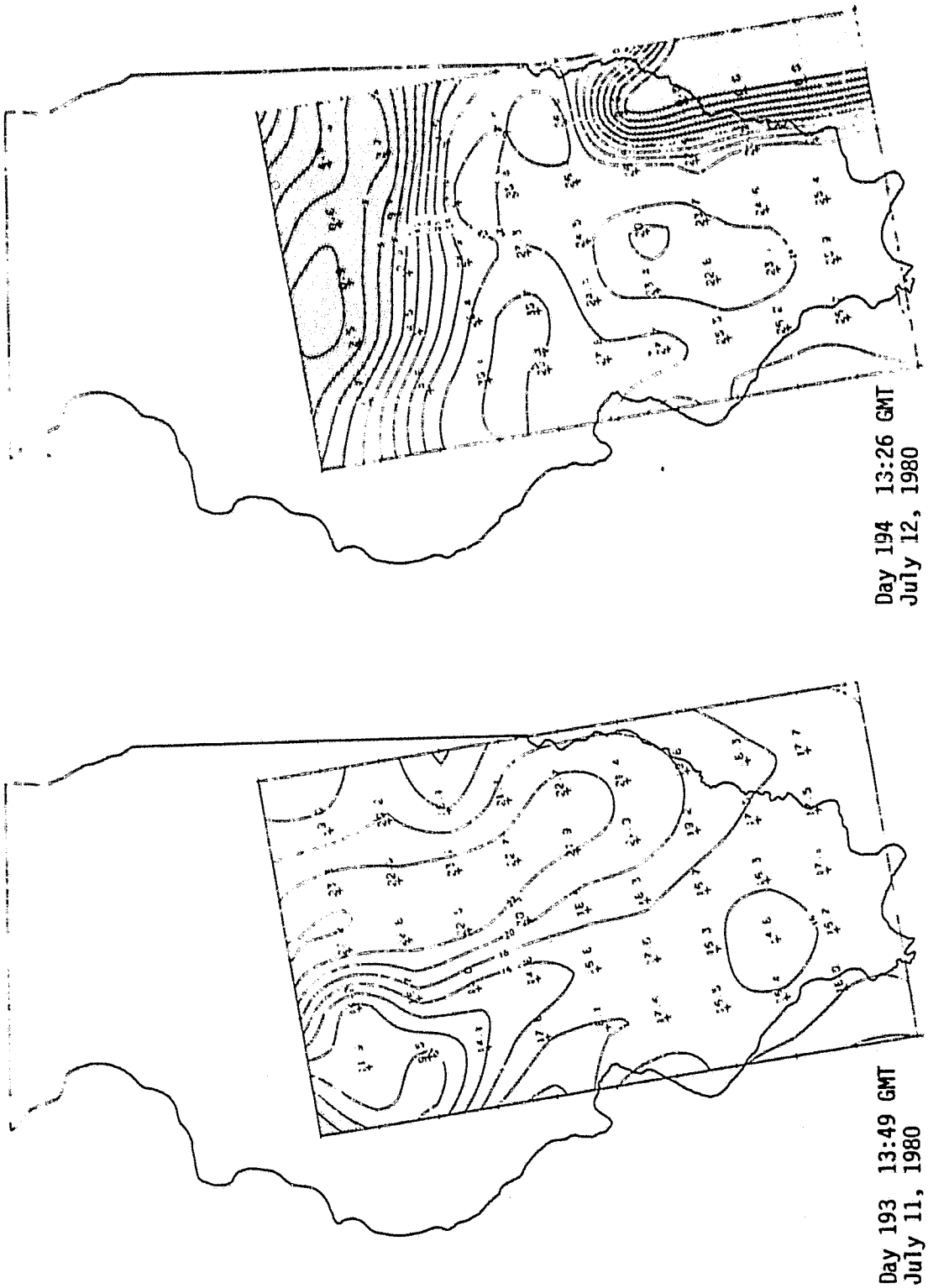

Figure A.1-1.- Continued.

ORIGINAL PAGE IS
OF POOR QUALITY

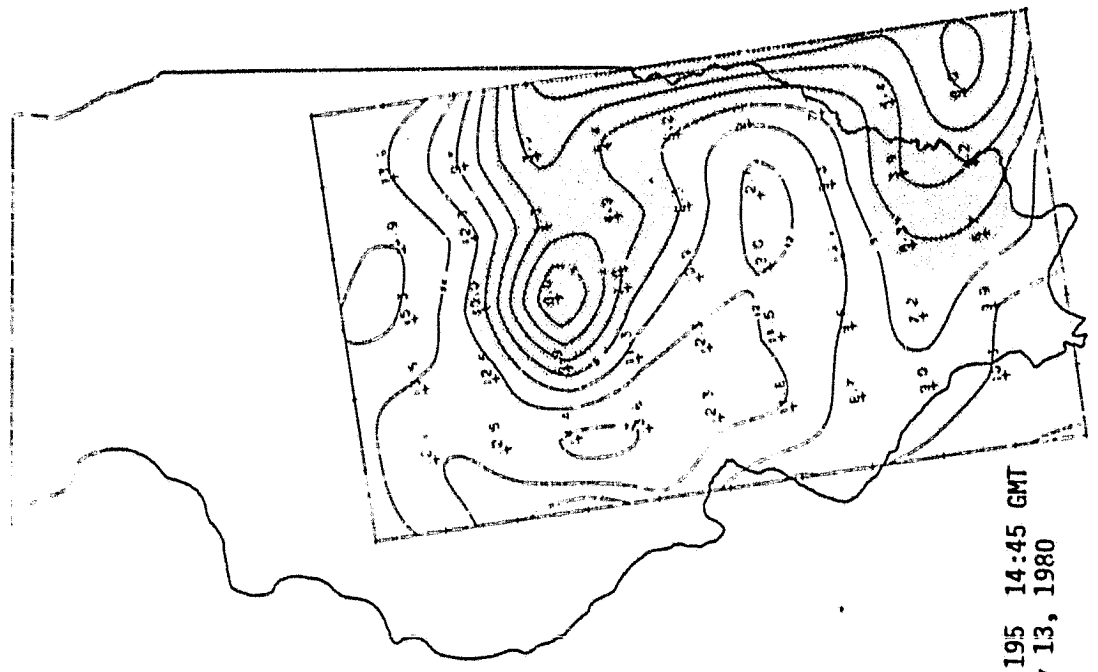

Day 195 14:45 GMT
July 13, 1980

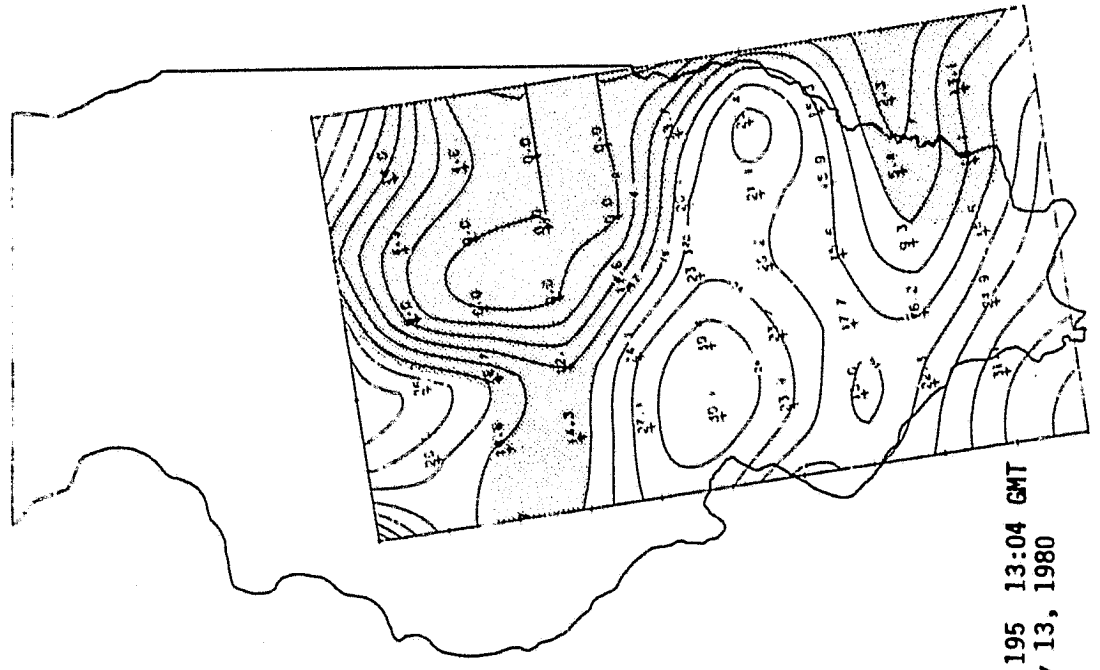

Day 195 13:04 GMT
July 13, 1980

Figure A.1-1.- Continued.

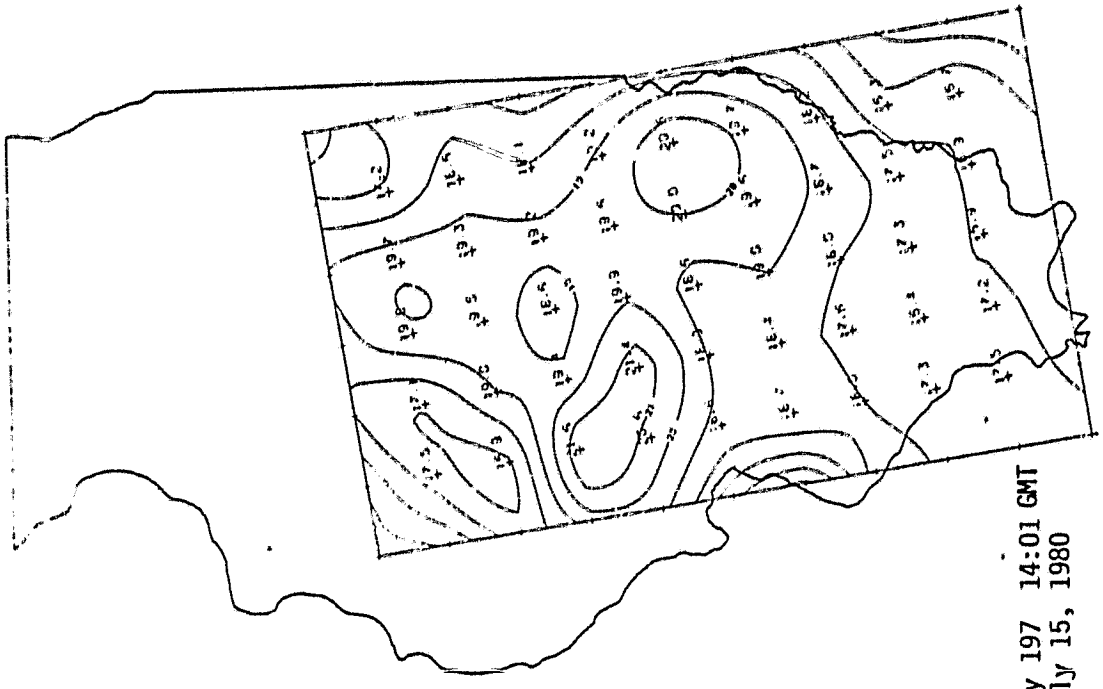

Day 197 14:01 GMT
July 15, 1980

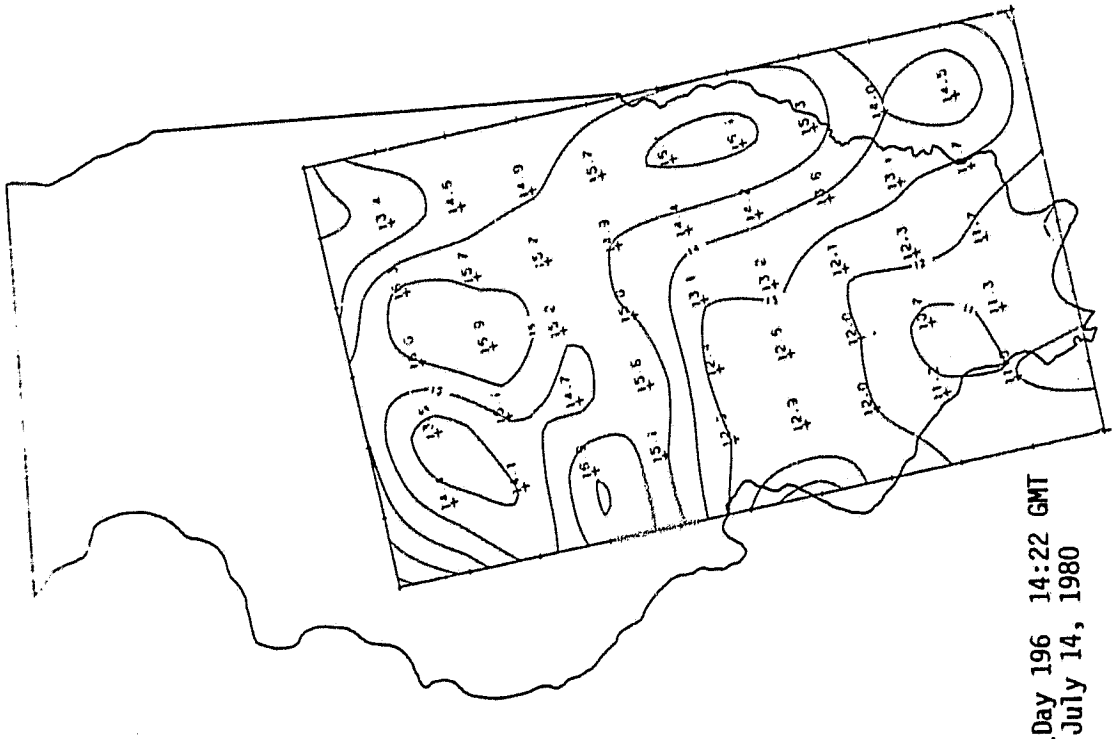

Day 196 14:22 GMT
July 14, 1980

Figure A.1-1.- Continued.

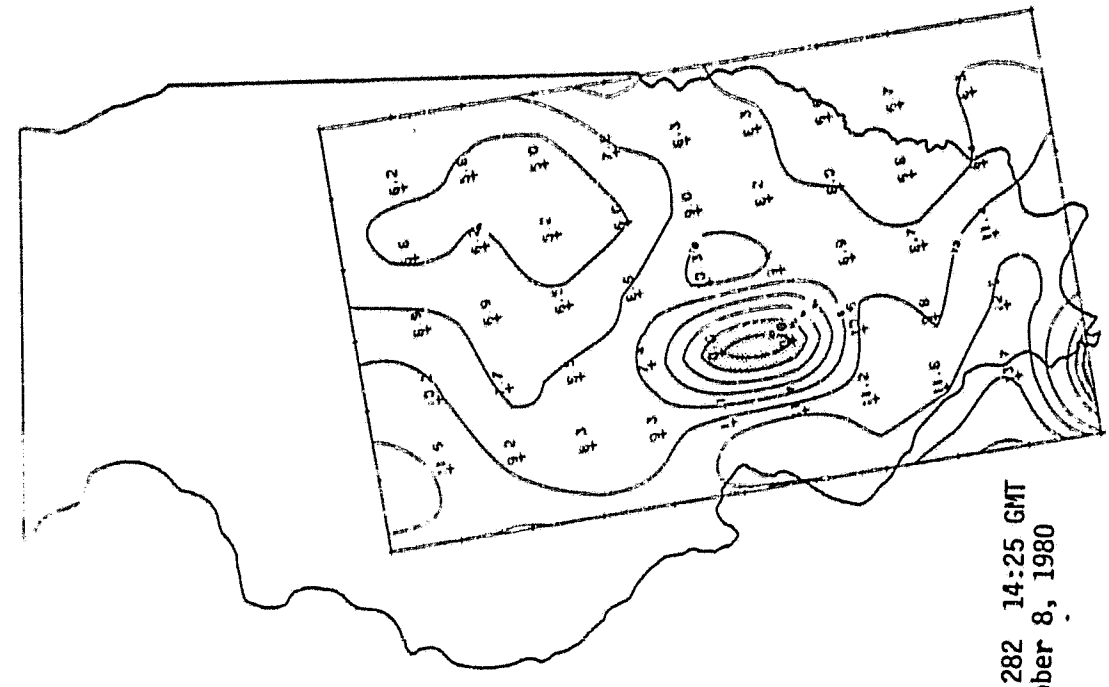

Day 282 14:25 GMT
October 8, 1980

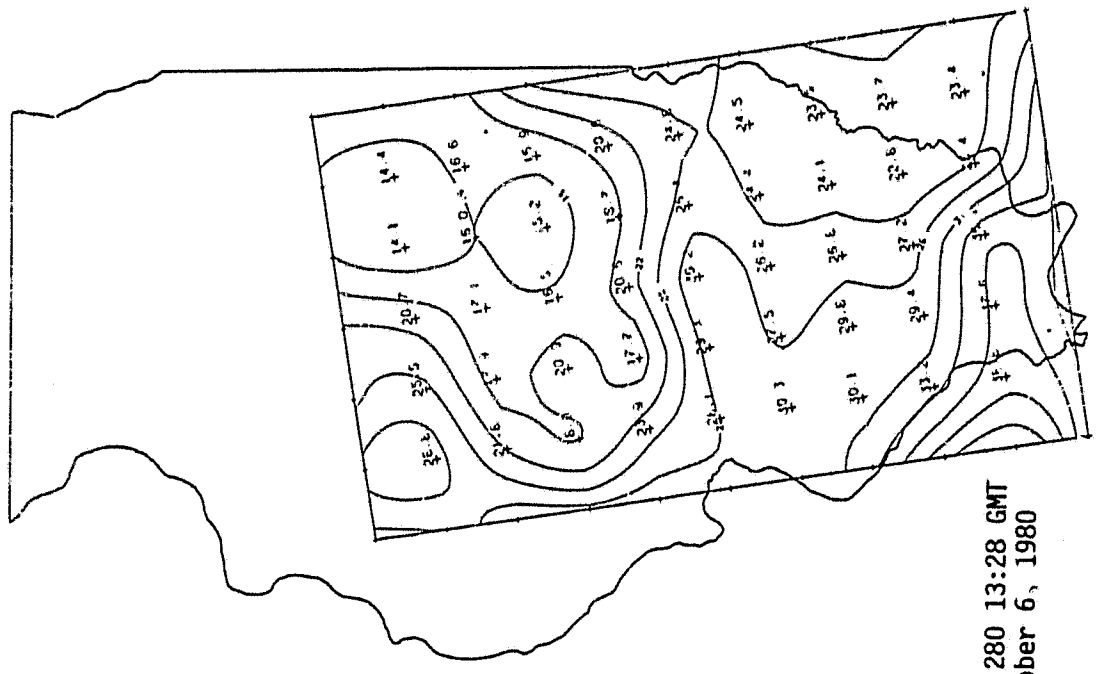

Day 280 13:28 GMT
October 6, 1980

Figure A.1-1.- Continued.

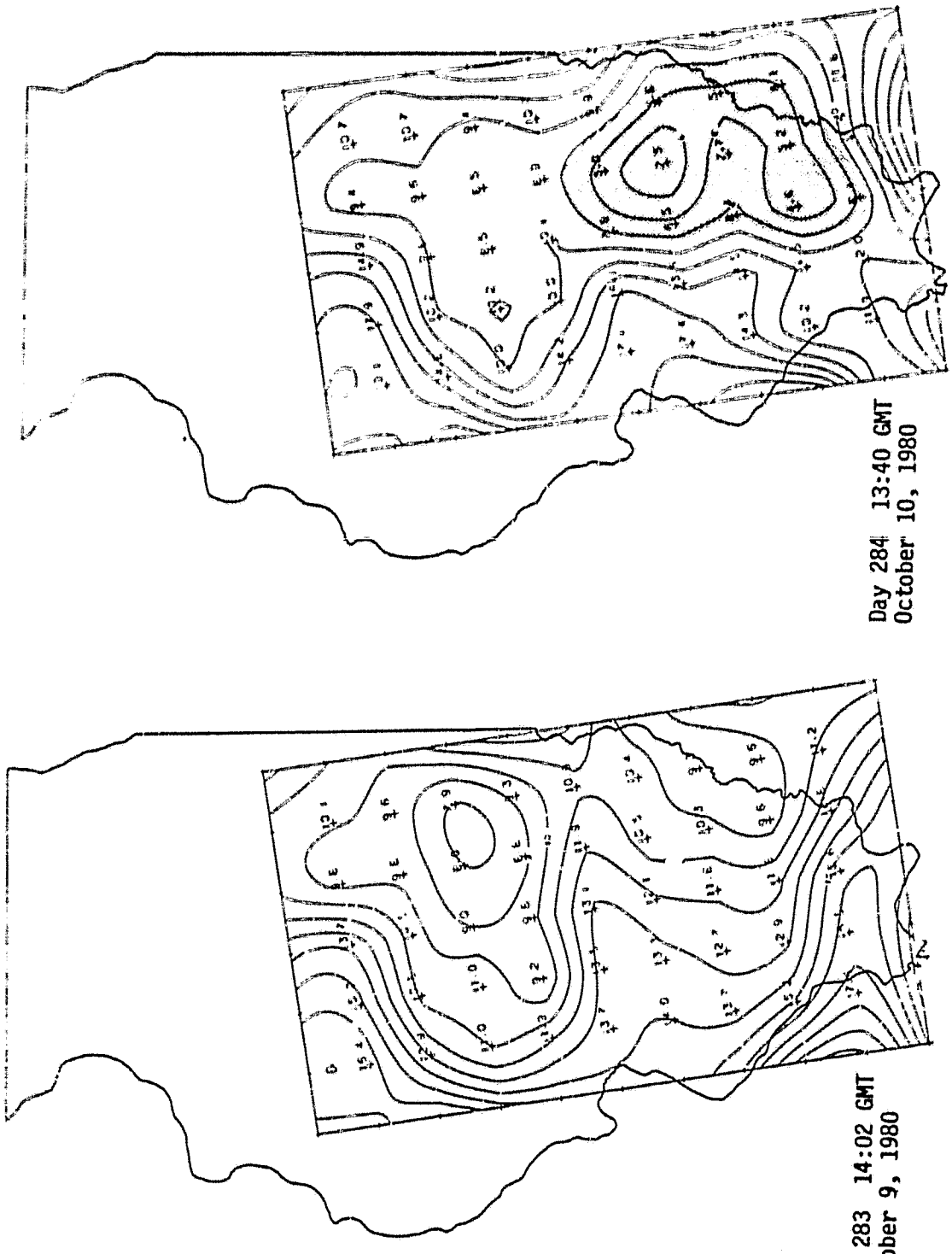

Figure A.1-1.- Concluded.

A.2 SCATTERPLOTS

The five scatterplots which appear in this section are representative of the 33 scatterplots which were generated for this study. Figures A.2-1 and A.2-2 were produced from July data and figures A.2-3 through A.2-5 from October data.

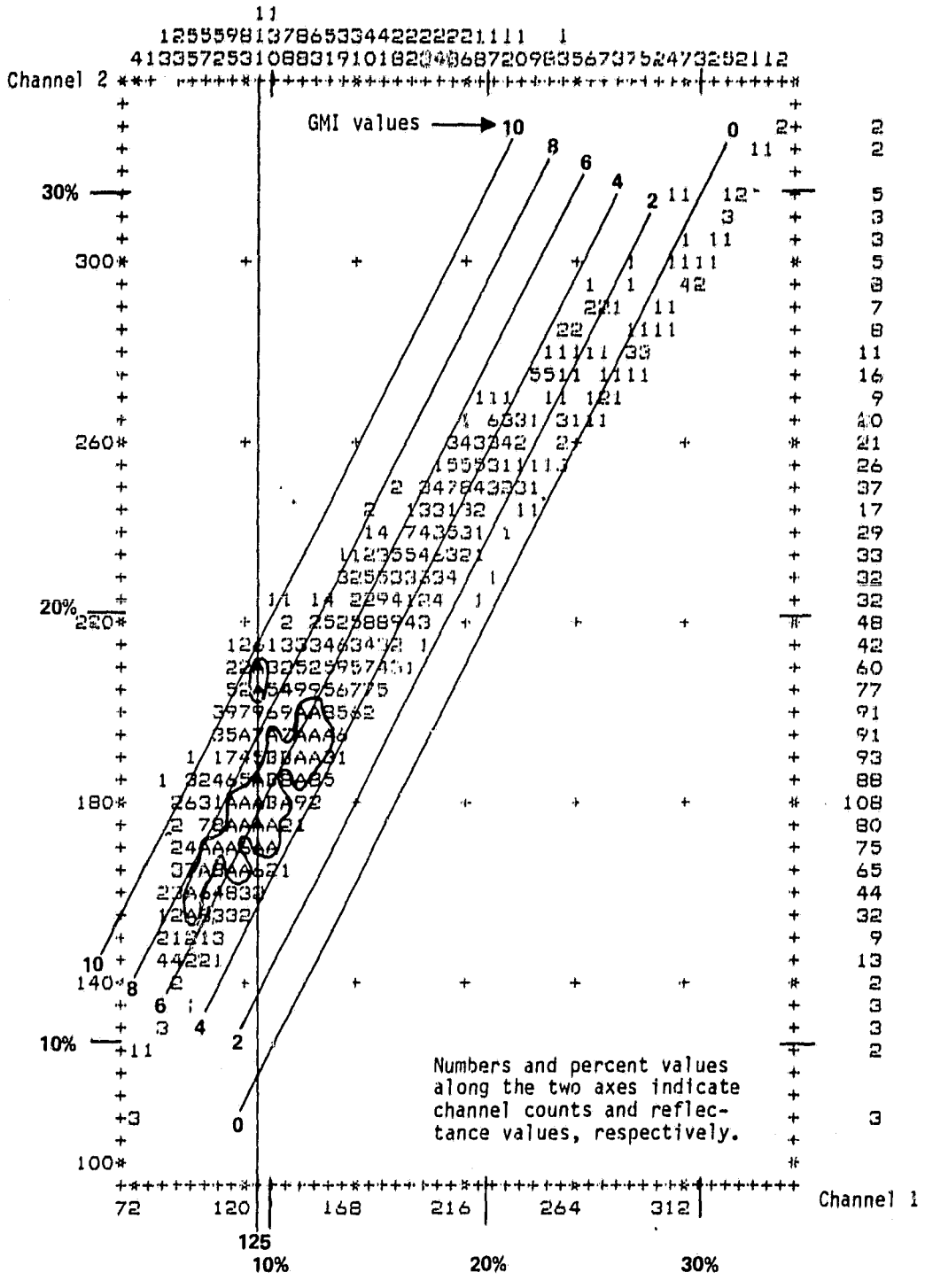

Figure A.2-1.- Scatterplot for i,j coordinates (235, 372) with 1355 pixels. [Julian day 191]

ORIGINAL PAGE IS
OF POOR QUALITY

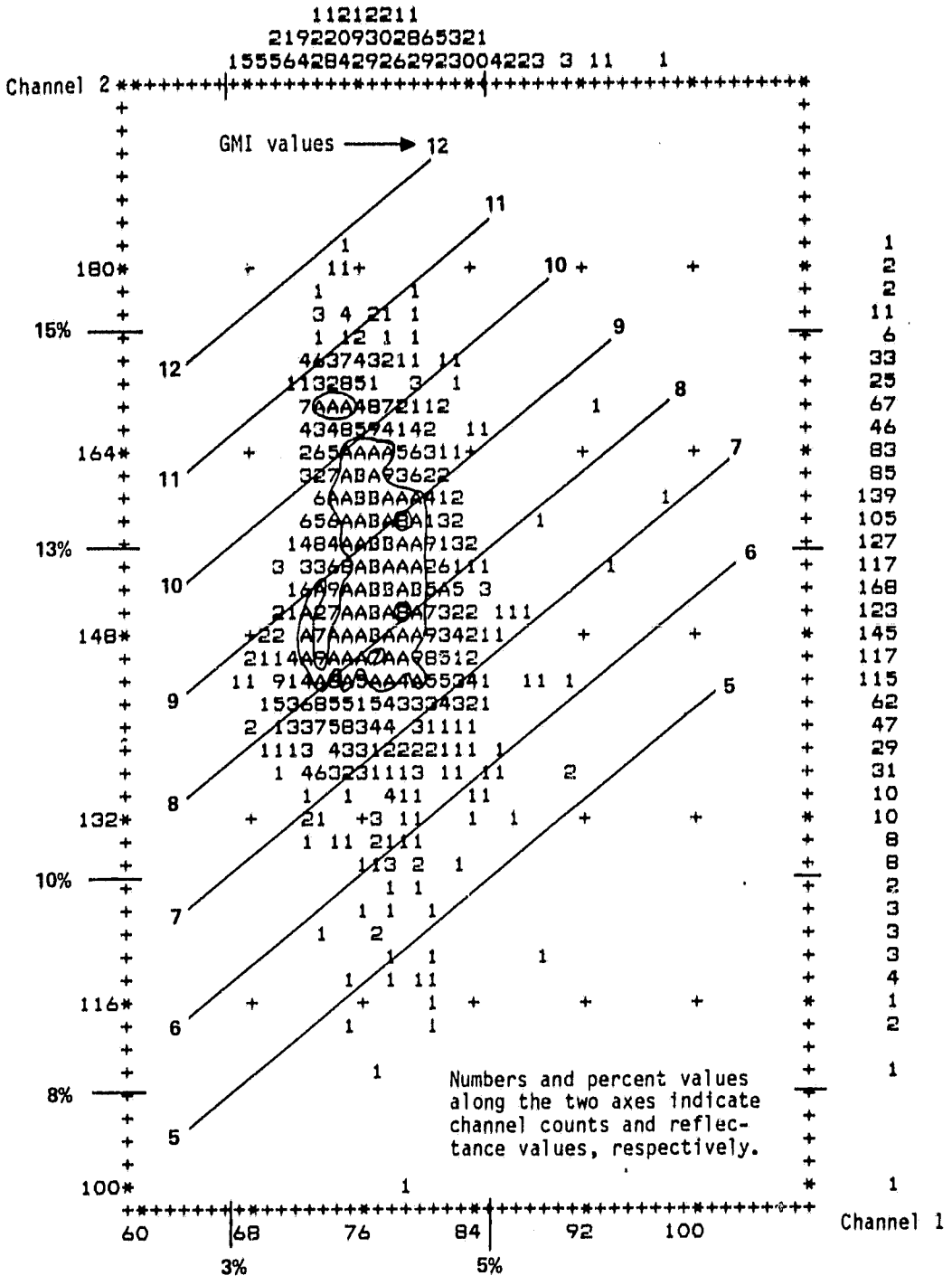

Figure A.2-2.- Scatterplot for i,j coordinates (235, 372) with 1742 pixels. [Julian day 196]

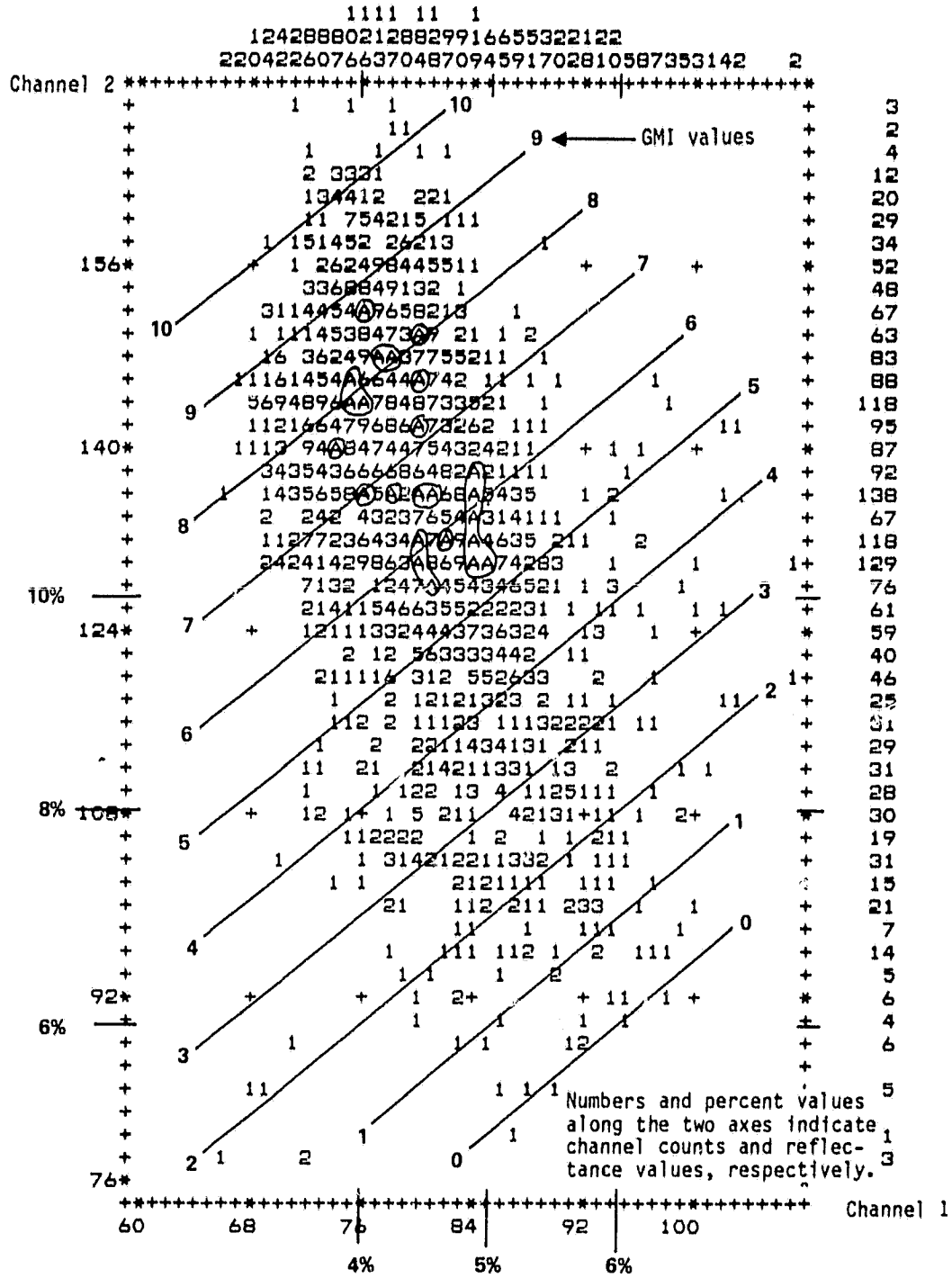

Figure A.2-3.- Scatterplot for i,j coordinates (235, 375) with 1942 pixels. [Julian day 197]

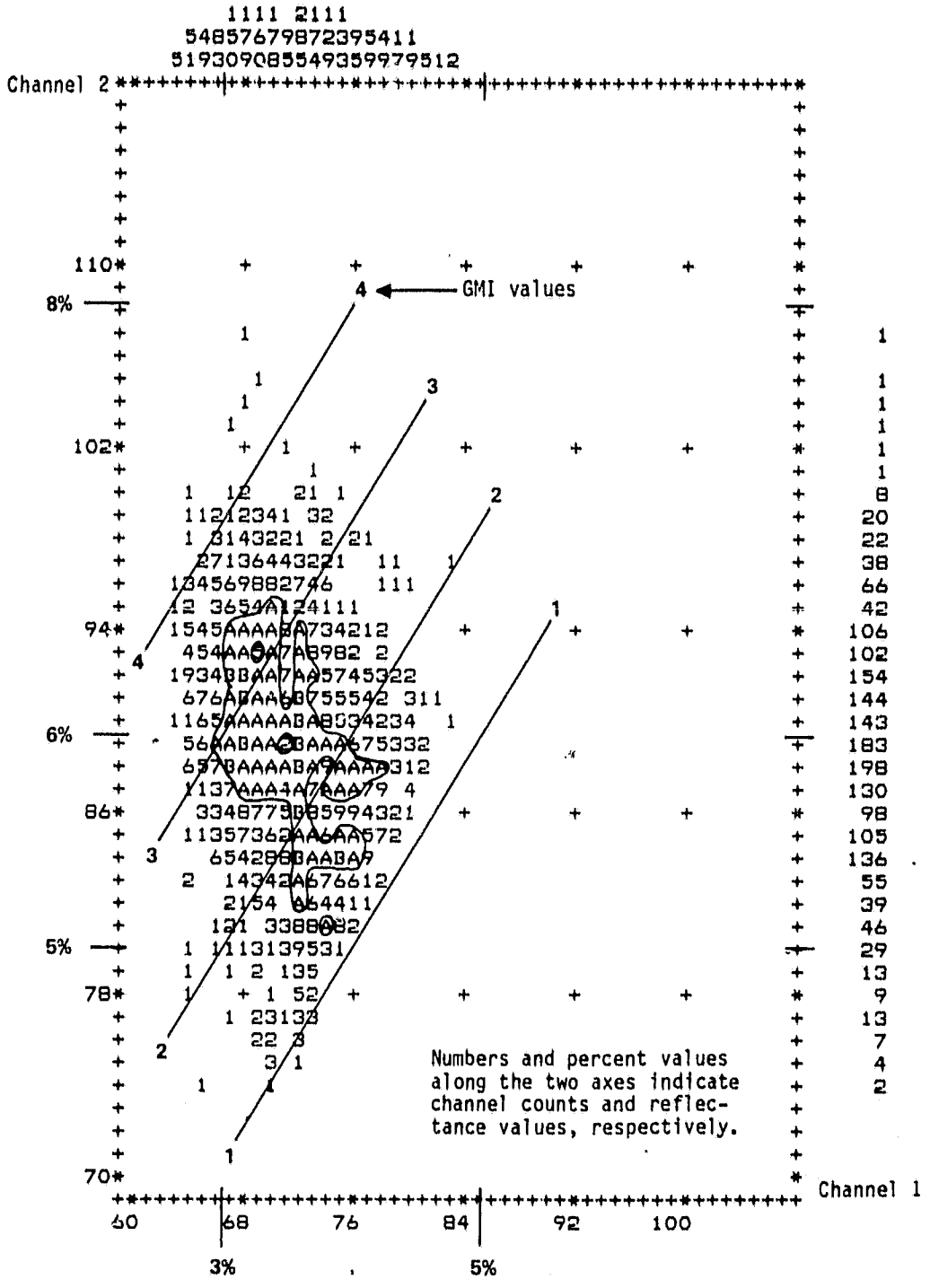

Figure A.2-4.- Scatterplot for i,j coordinates (235, 372) with 1918 pixels. [Julian day 283]

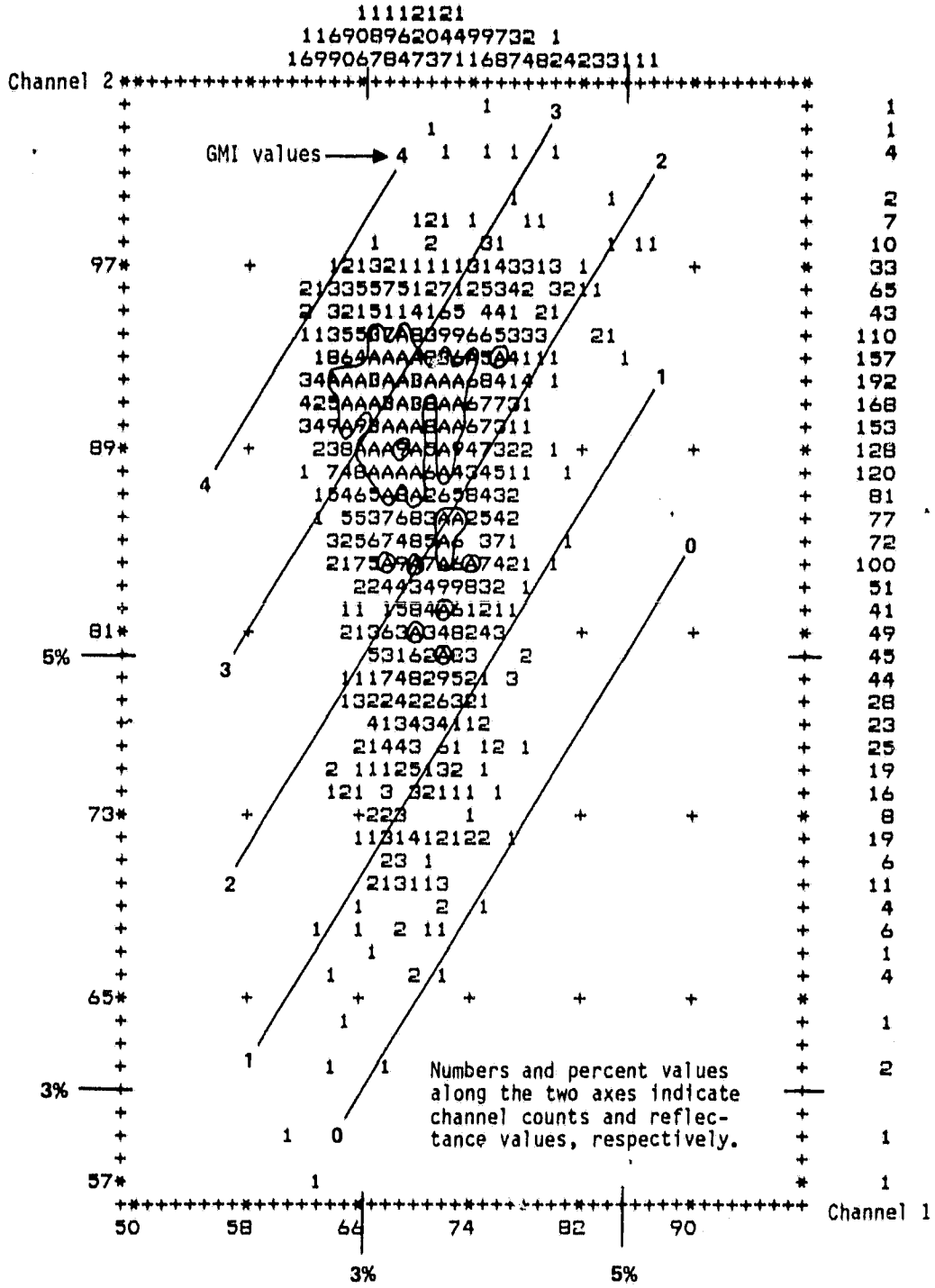

Figure A.2-5.- Scatterplot for i,j coordinates (235, 375) with 1929 pixels. [Julian day 283]

A.3 TRANSECTIONS

The transections (or cross sections) which appear in this appendix were produced from the actual raw-pixel values from channels 1 and 2.

Figure A.3-1 shows maximum GMI values (scale to the left) and maximum corrected GMI values (scale to the right) for each 50 pixels.

Figure A.3-2 shows the largest channel counts for each 50 pixels. A value of 125 for channel 1, which was considered the lower cutoff for clouds, appears on the graph as a dark horizontal line. Any value plotted above this line indicates the presence of clouds.

Figure A.3-3 shows a comparison of data acquired from two overflights over the same surface at different times.

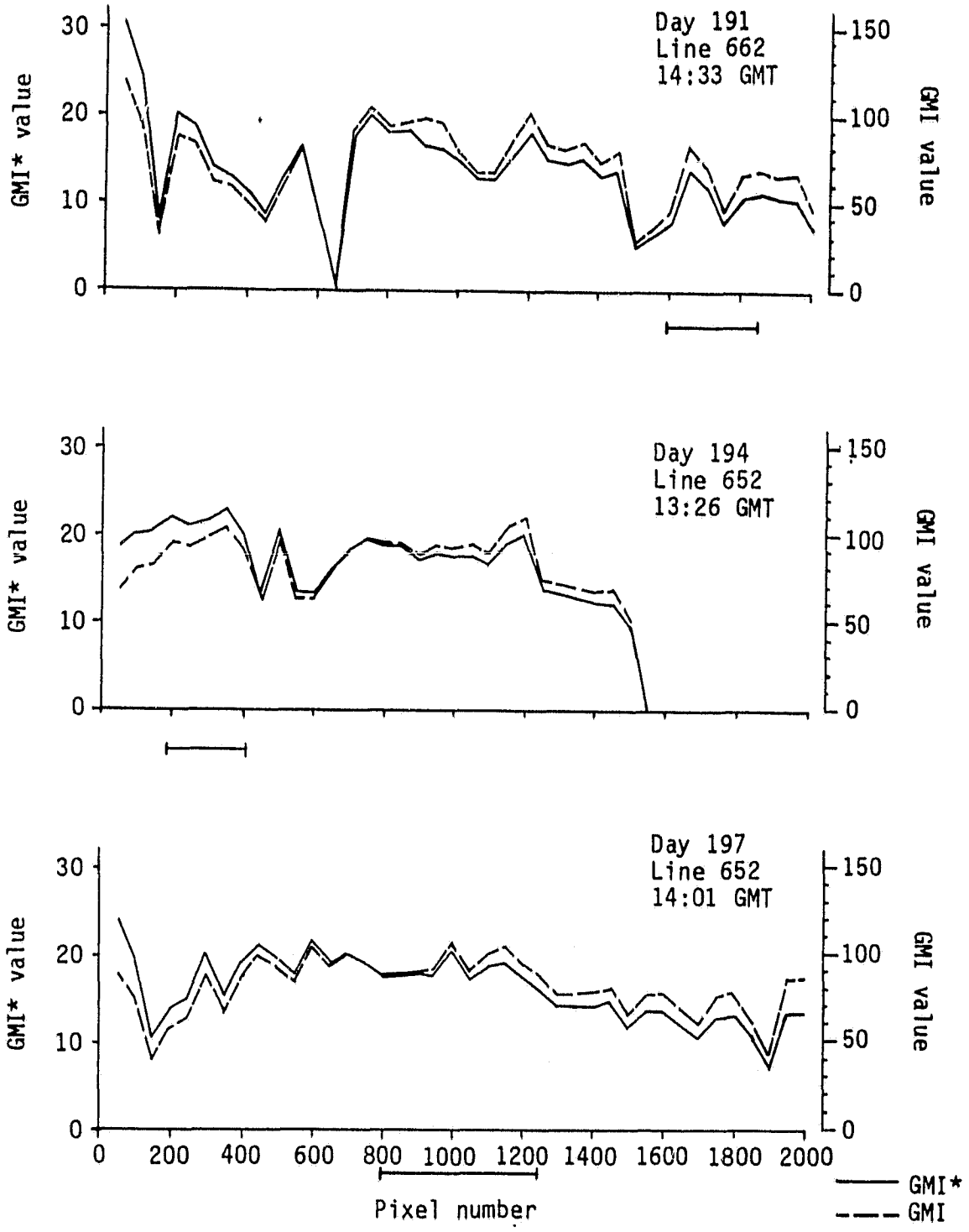

Figure A.3-1.- Maximum GMI and maximum GMI* values for each 50 pixels.

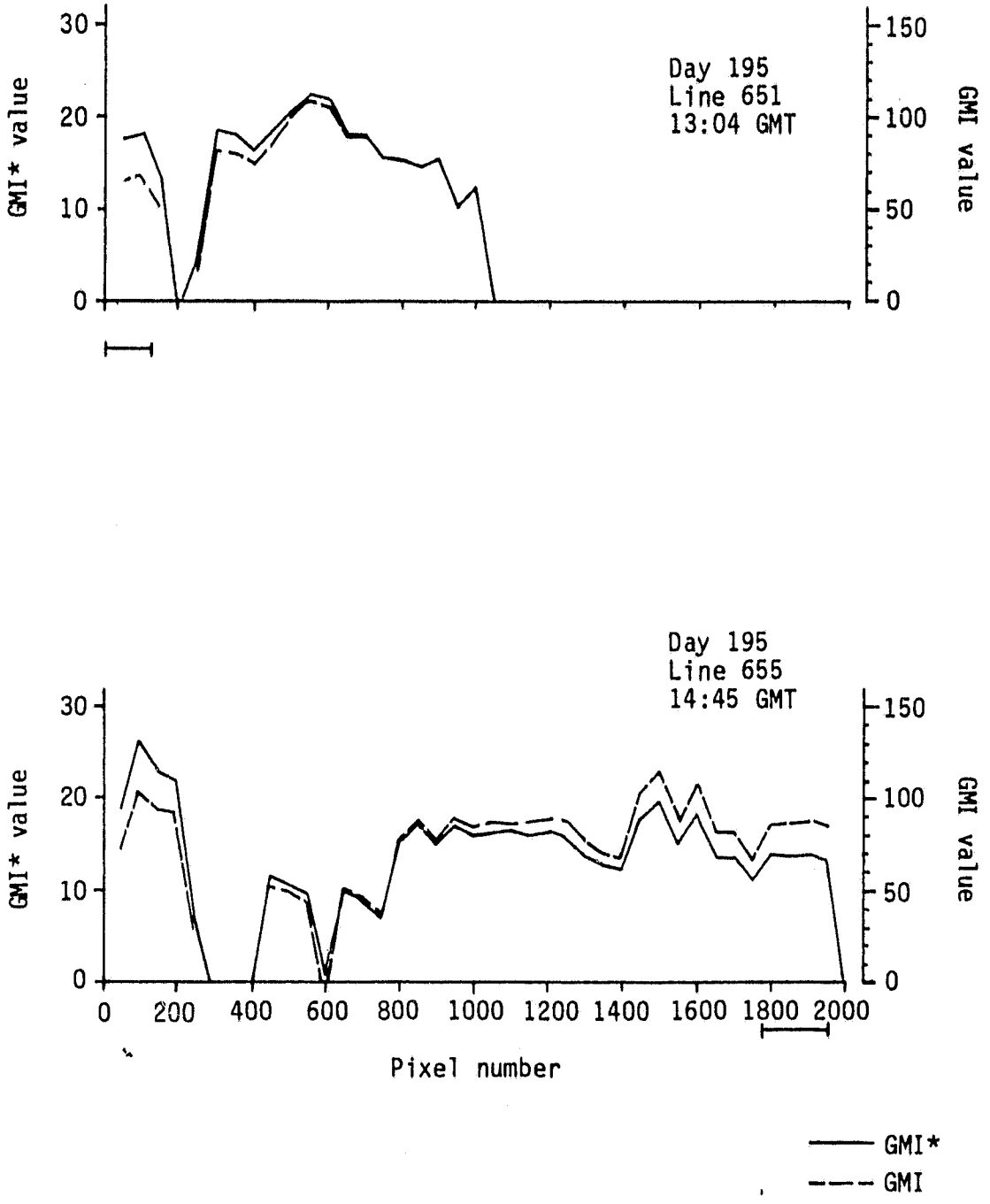

Figure A.3-1.- Continued.

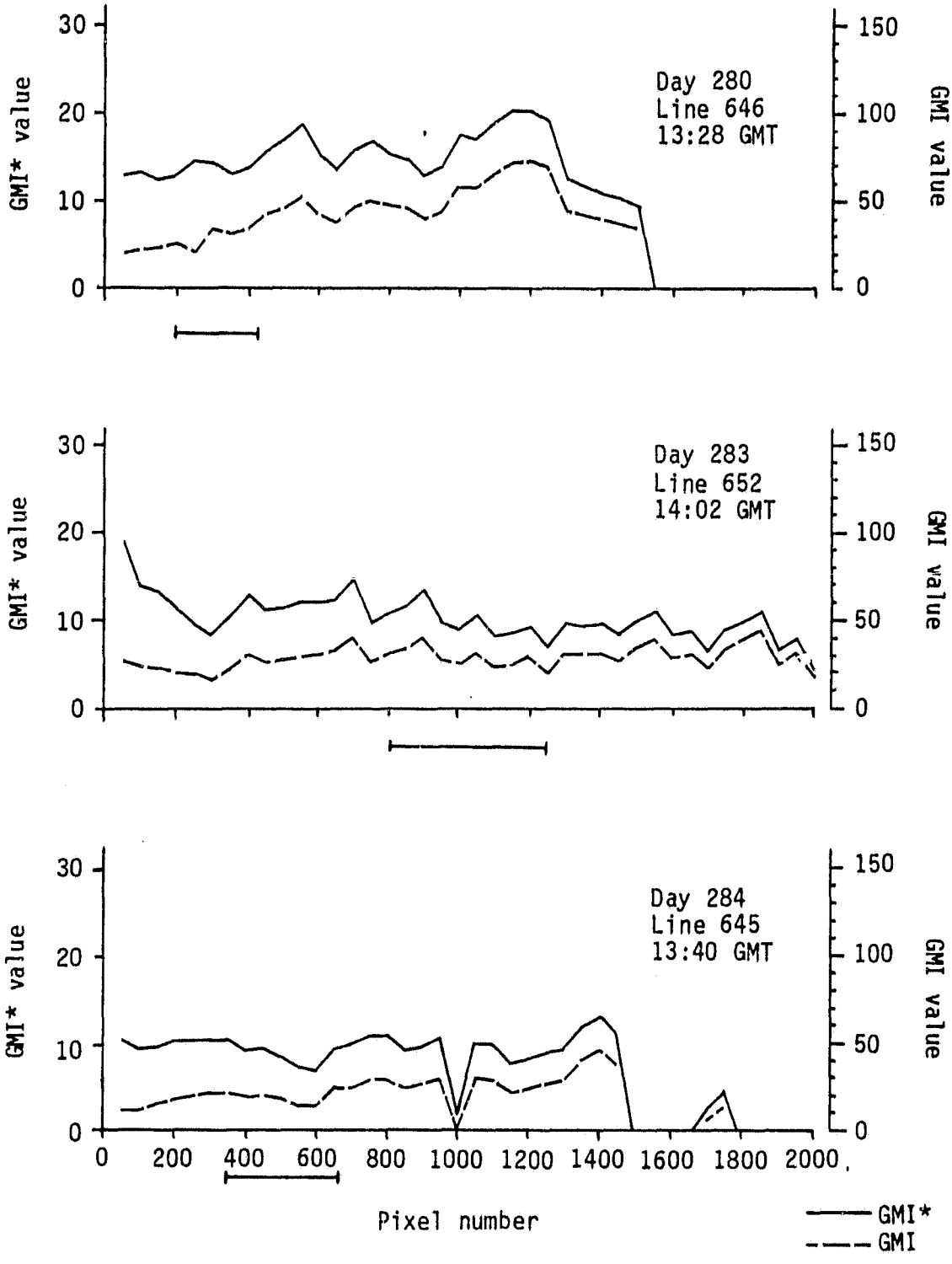

Figure A.3-1.- Concluded.

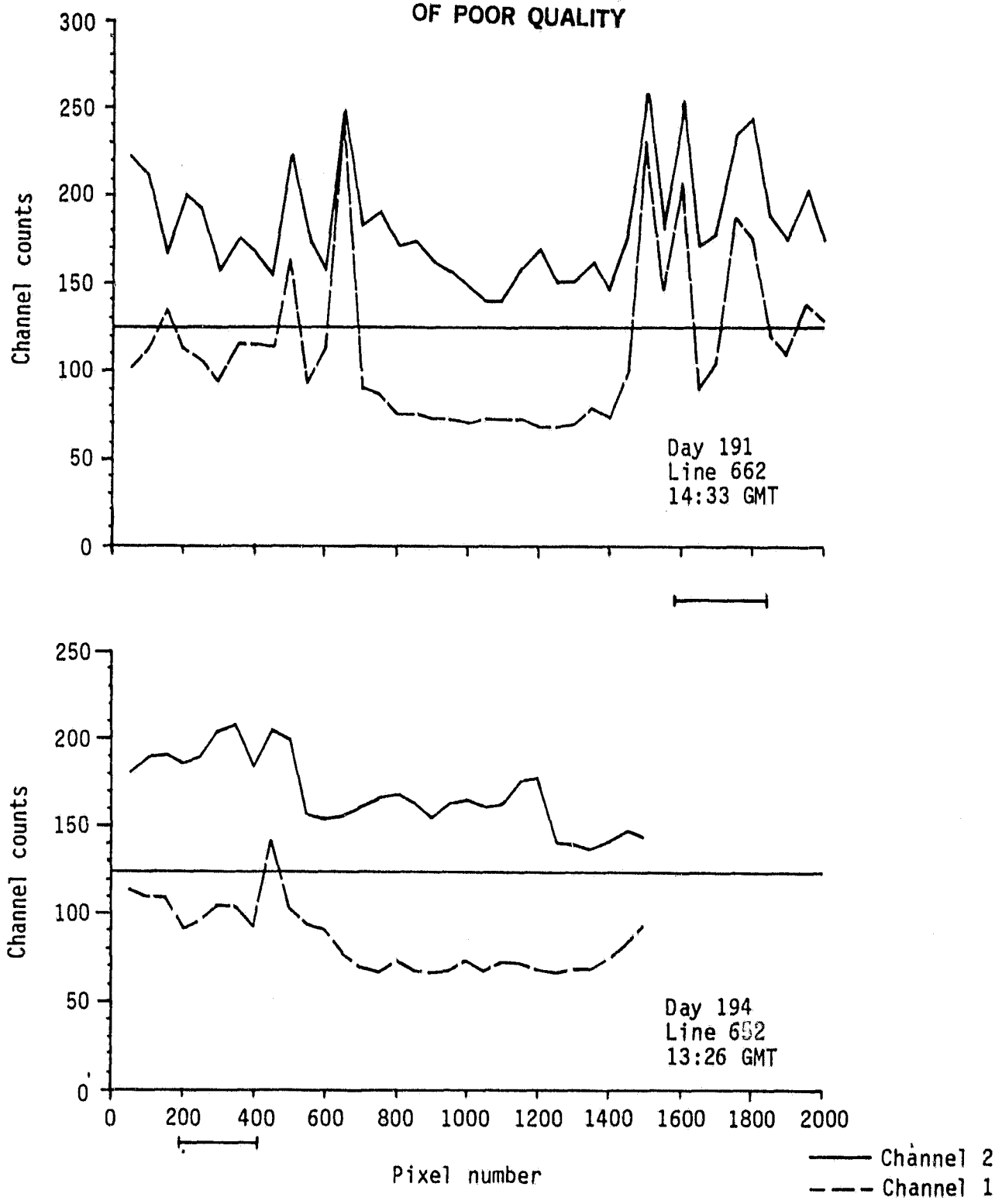

Figure A.3-2.- Largest channel counts for each 50 pixels.

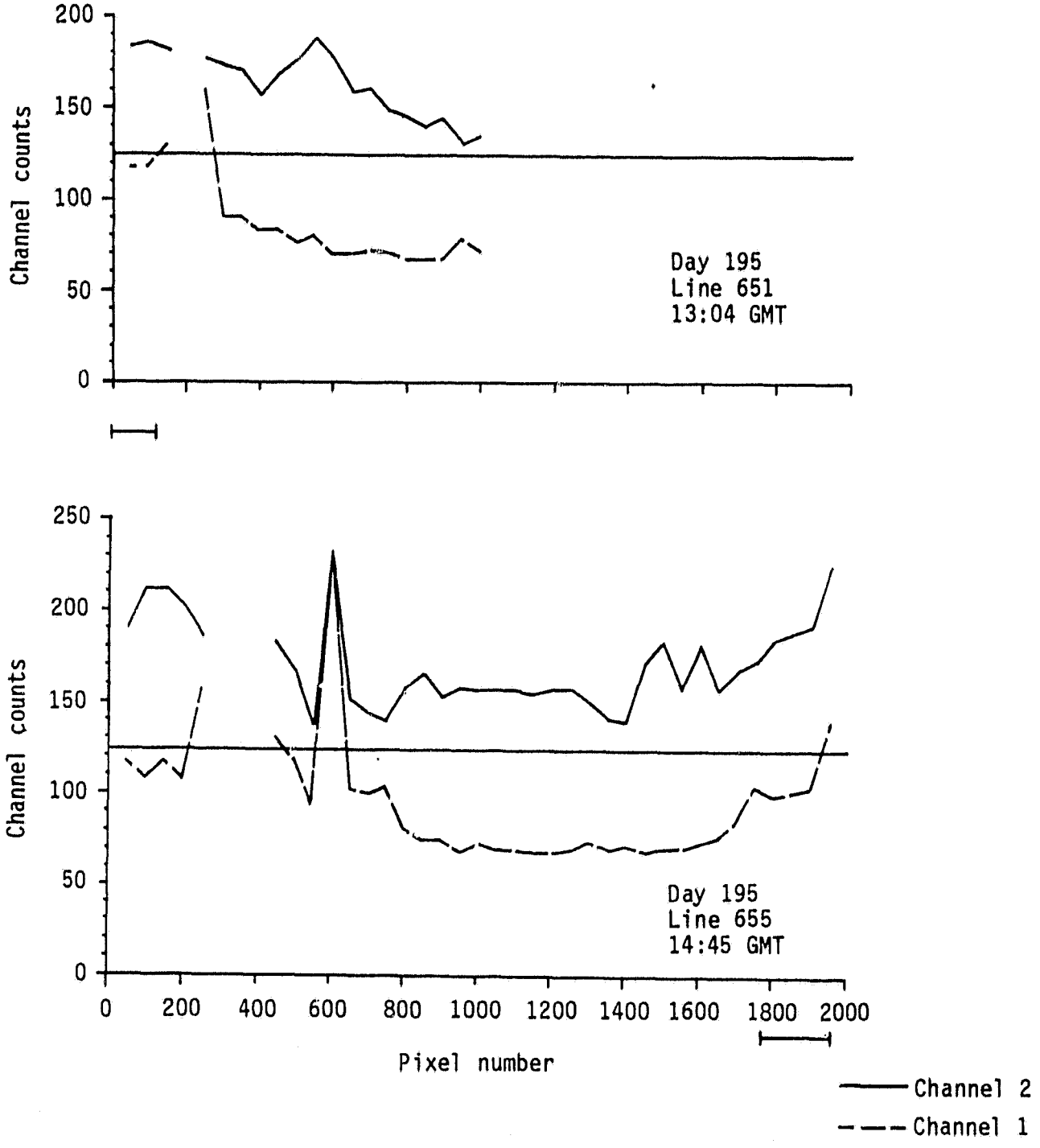

Figure A.3-2.- Continued.

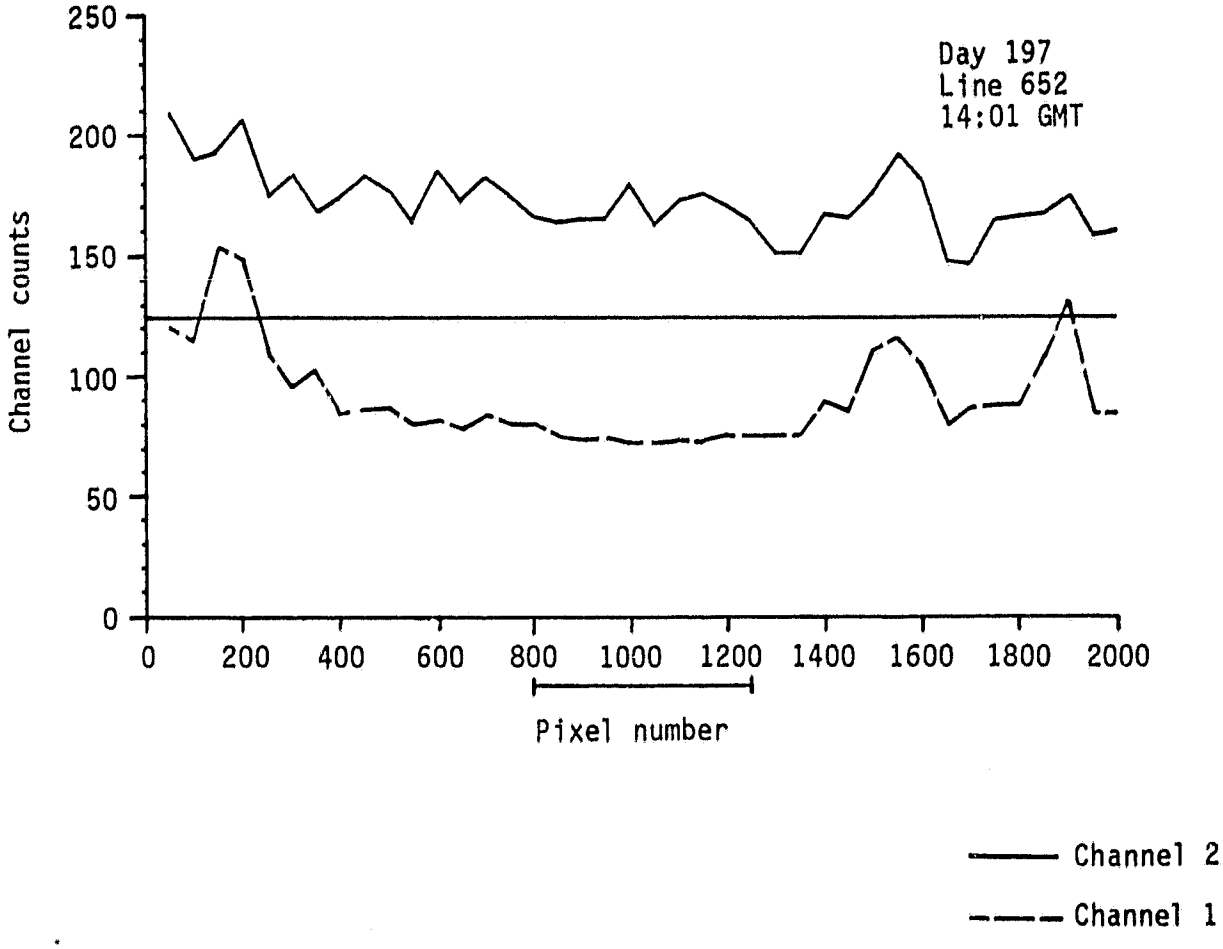

Figure A.3-2.- Continued.

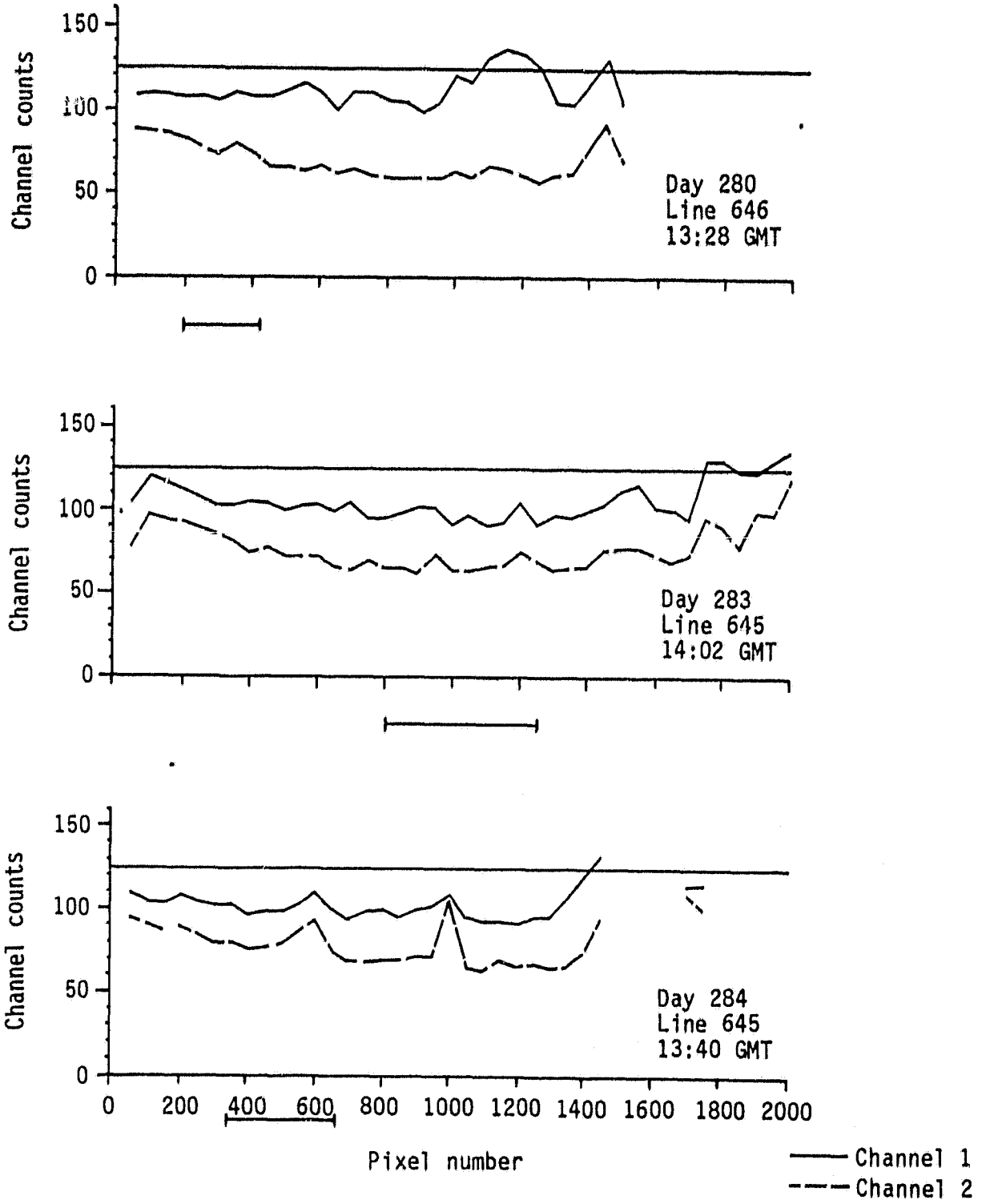

Figure A.3-2.- Concluded.

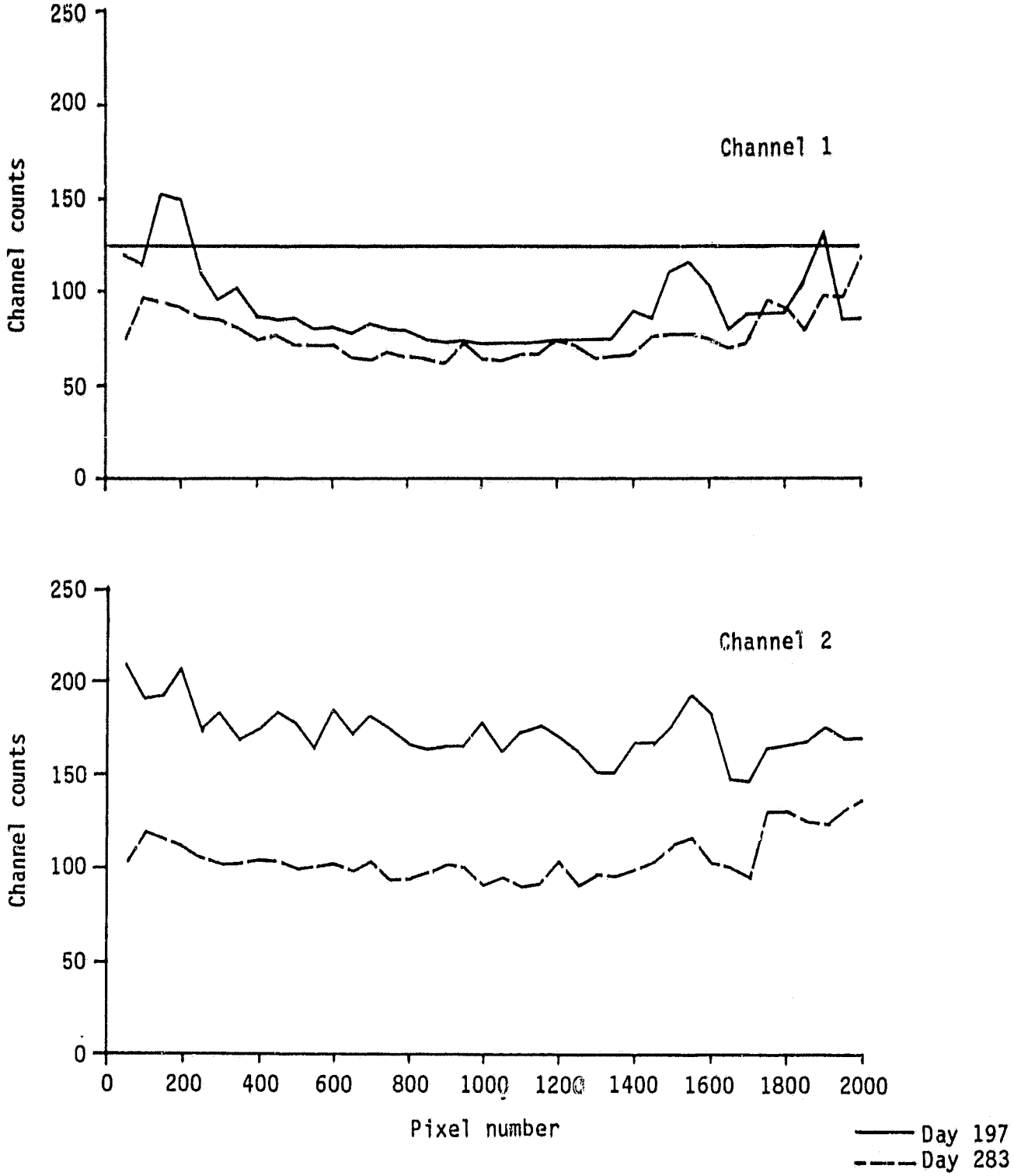

Figure A.3-3.- Comparison of data acquired from two overflights over the same surface at different times.

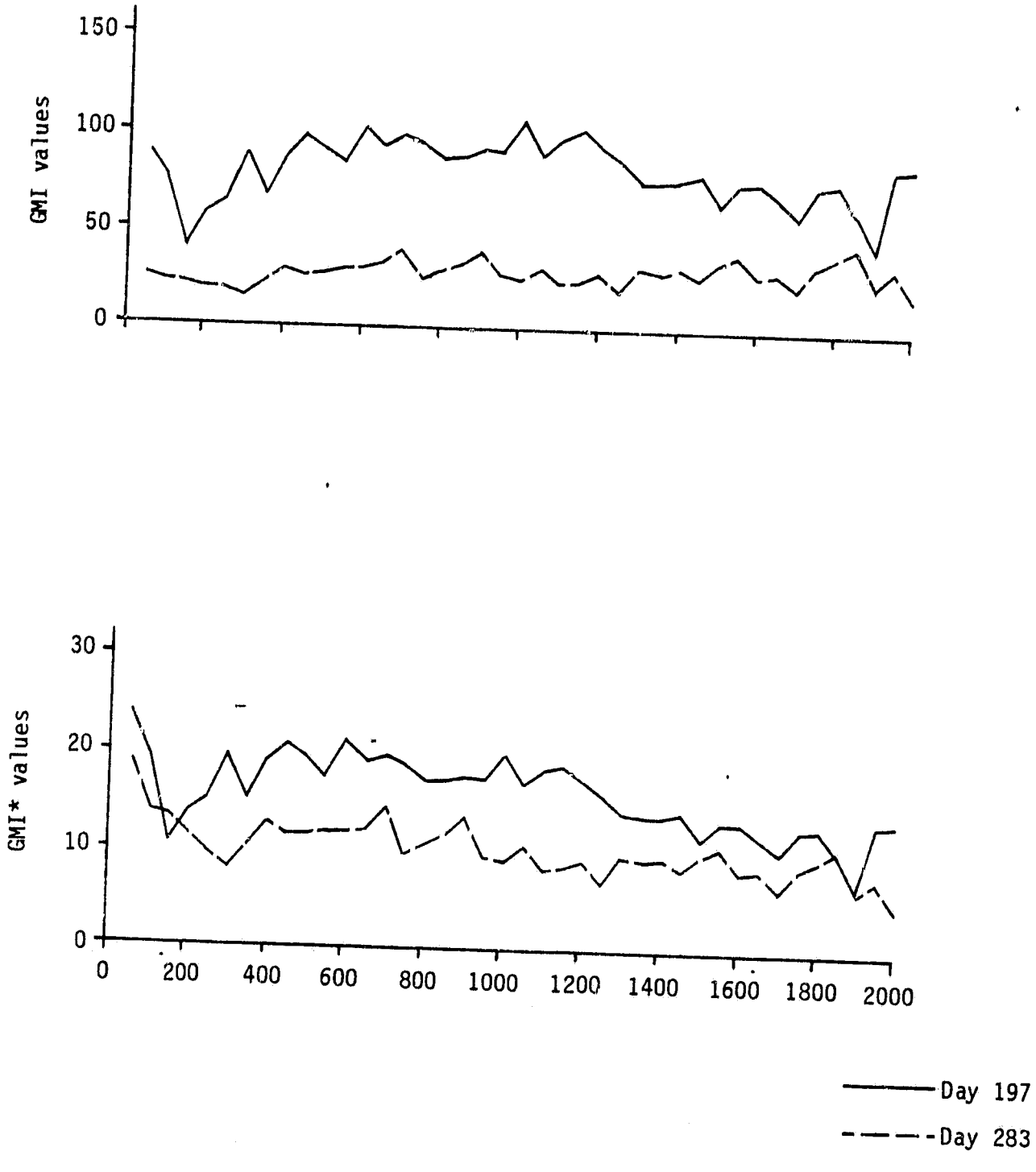

Figure A.3-3.- Concluded.

A.4 PRECIPITATION ANALYSIS

The figures in this section show the amounts of precipitation received in the areas delineated on the map of the target area for the dates indicated.

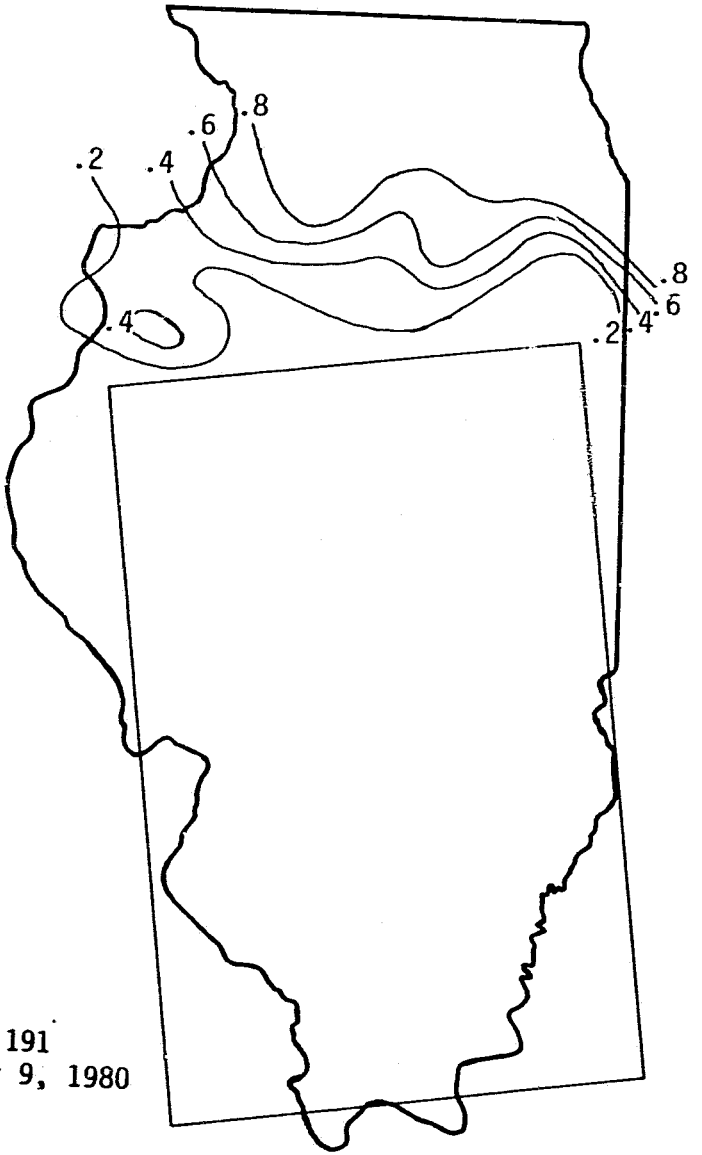

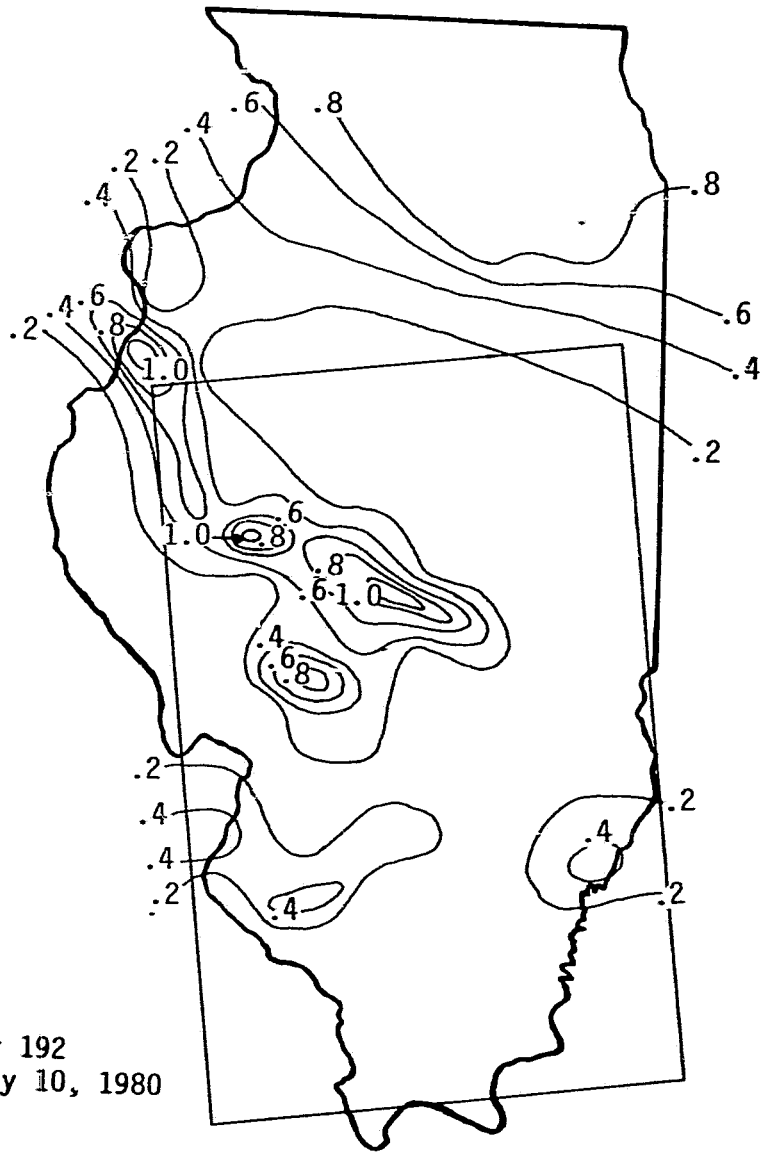

Figure A.4-1.- Precipitation amounts (in inches) received in the target area.

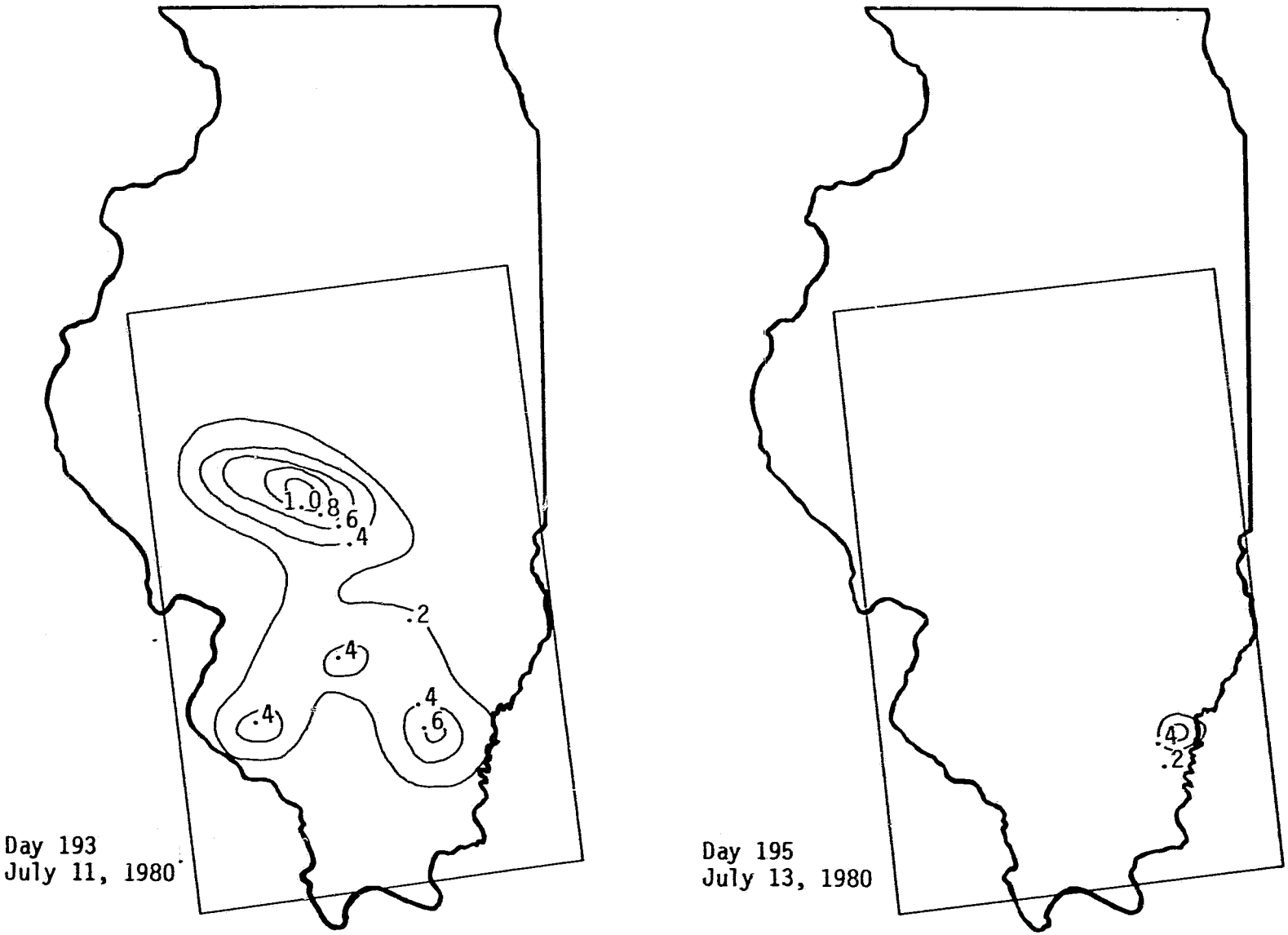

Figure A.4-1.- Continued.

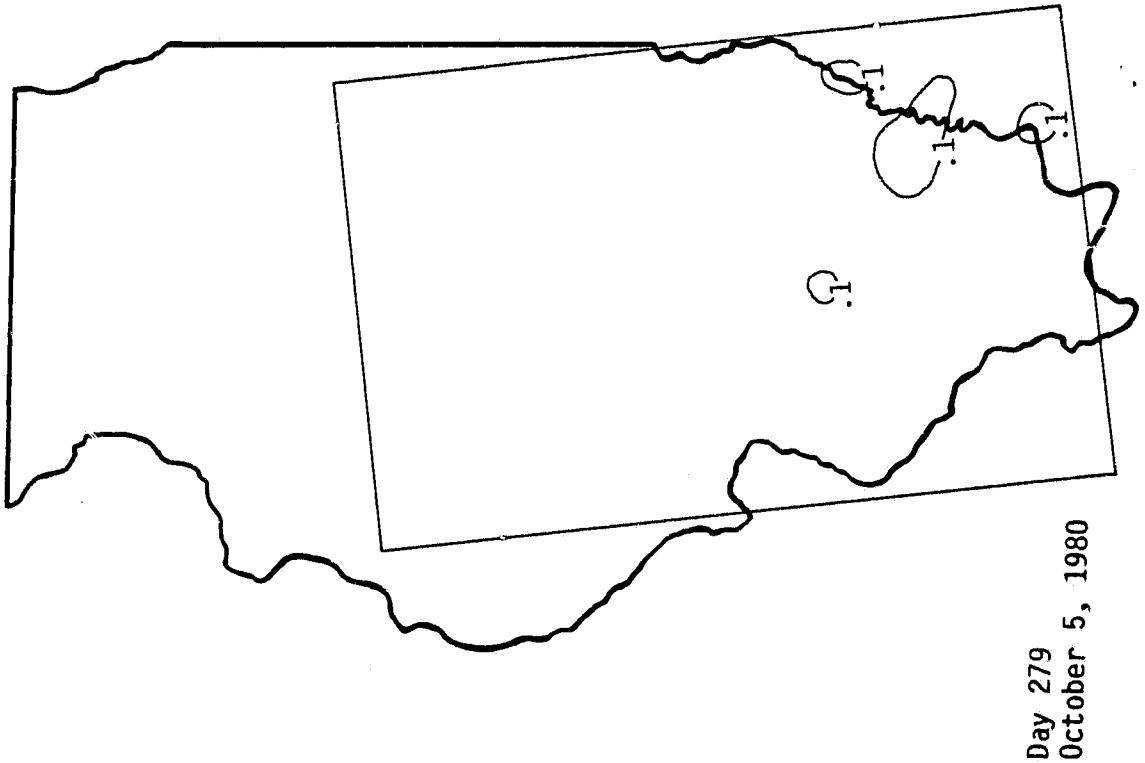

Figure A.4-1.- Concluded.

APPENDIX B

LIST OF COMPUTER PROGRAMS

APPENDIX B

LIST OF COMPUTER PROGRAMS

The following are programs used on the scene processing unit at the Agena building, 1050 Bay Area Boulevard, Houston, Texas.

1. LACREG
2. SAMPLE
3. PIXCAL
4. LACVIN
5. SCAT3

APPENDIX C

LIST OF DATA TAPES AND FILES

Bin no.	Tape ID	Date	Pixel range	GMT
027	LAC027	D80191	1545-1865	14:33
		D80191	(too far east)	
028	LAC028	D80191	(too far east)	
		D80192	985-1505	14:11
029	LAC029	D80192	(too far south)	
		D80195	10-125	13:04
030	LAC030	D80195	(too far east)	
		D80195	1785-1985	14:45
031	LAC031	D80196	1190-1700	14:22
		D80197	690-1200	14:01
032	LAC032	D80197	(too far south)	
		D80193	505-945	13:49
033	LAC033	D80193	(too far south)	
		D80194	185-465	13:26
034	LAC034	D80280	185-465	13:28
		D80282	(minimal data)	
035	LAC035	D80282	1305-1745	14:25
		D80283	785-1265	14:02
036	LAC036	D80283	(too far south)	
		D80284	160-670	13:40
037	LAC037	D80284	(too far south)	

APPENDIX D

SOLAR ZENITH-ANGLE CHARTS

APPENDIX D

SOLAR ZENITH-ANGLE CHARTS

The solar zenith-angle charts in this appendix show how solar zenith angle and pixel numbers change accross the target area on a specific day. The Julian day, date, and GMT of the data acquisition are indicated beside each chart. Pixel numbers are indicated by solid lines and solar zenith-angle values by broken lines.

For the charts made from October acquisitions, the solar angle values may be in error by 1° to 2°, possibly because of the solar declination value used by the satellite.

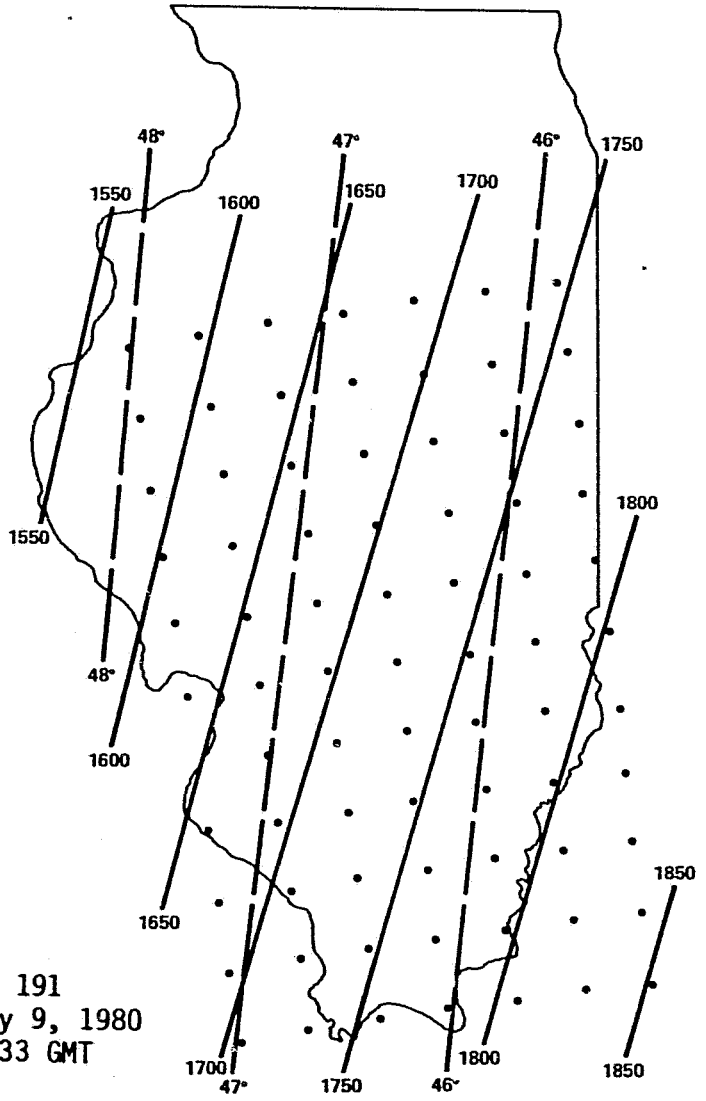

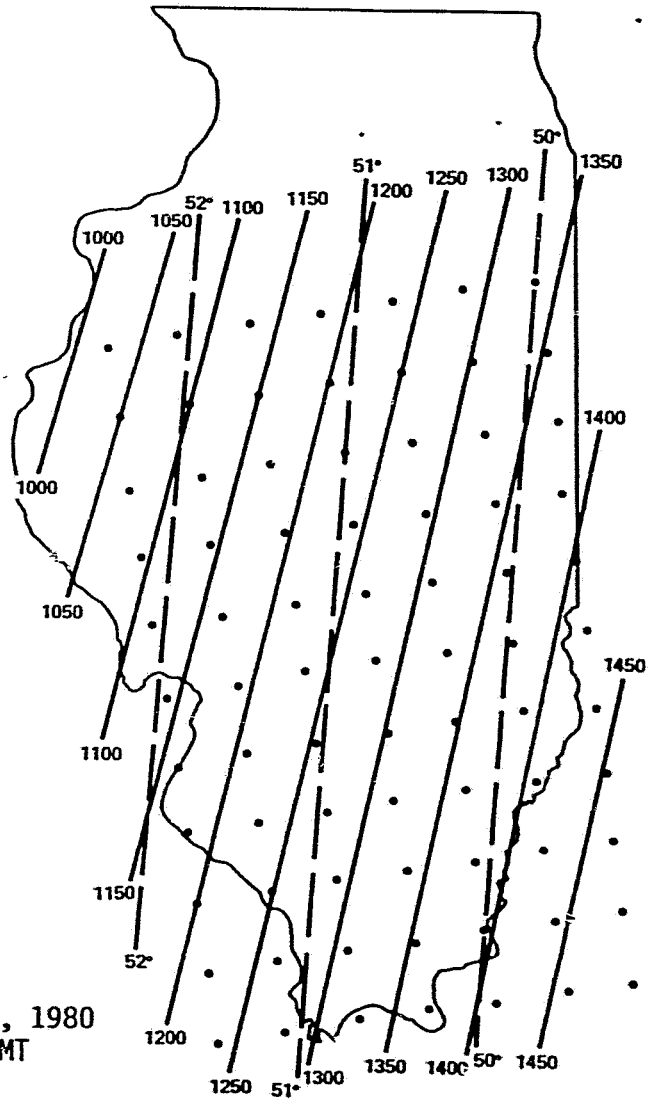

Figure D-1.- Solar zenith angle and pixel number chart.

ORIGINAL PAGE IS
OF POOR QUALITY

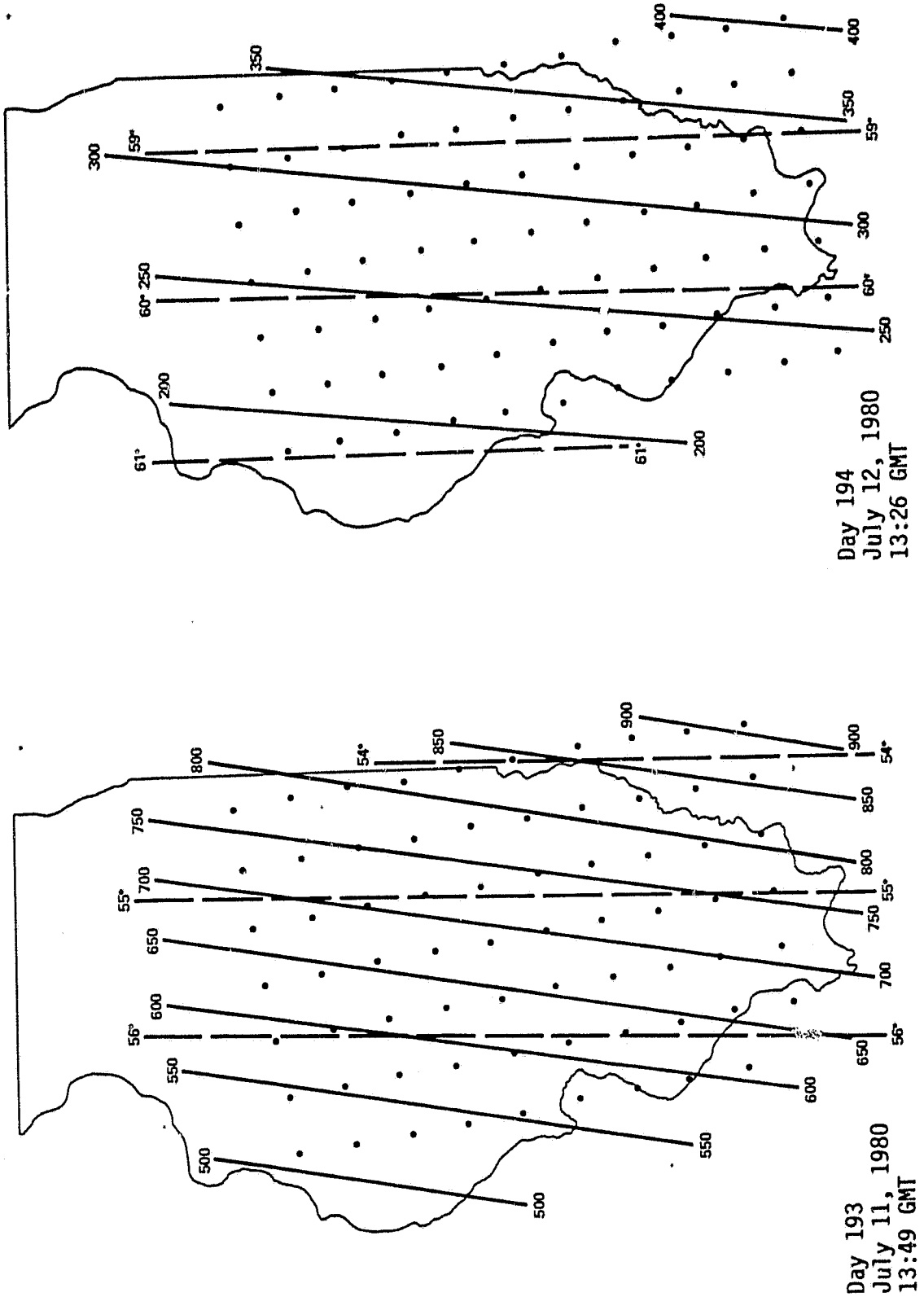

Figure D-1.- Continued.

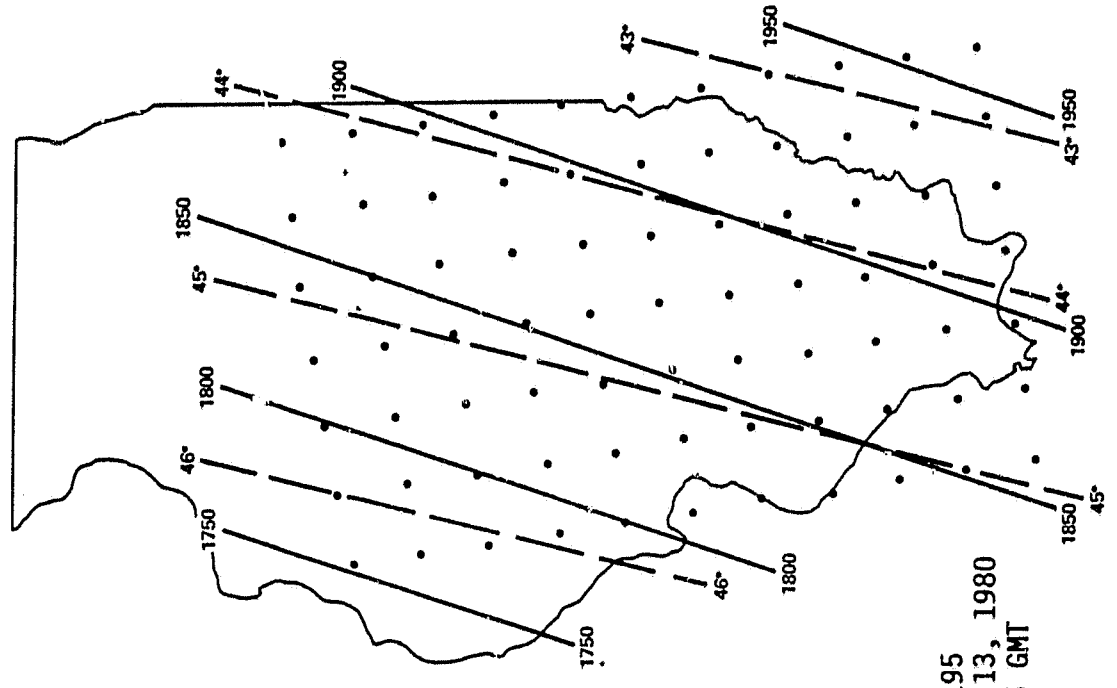

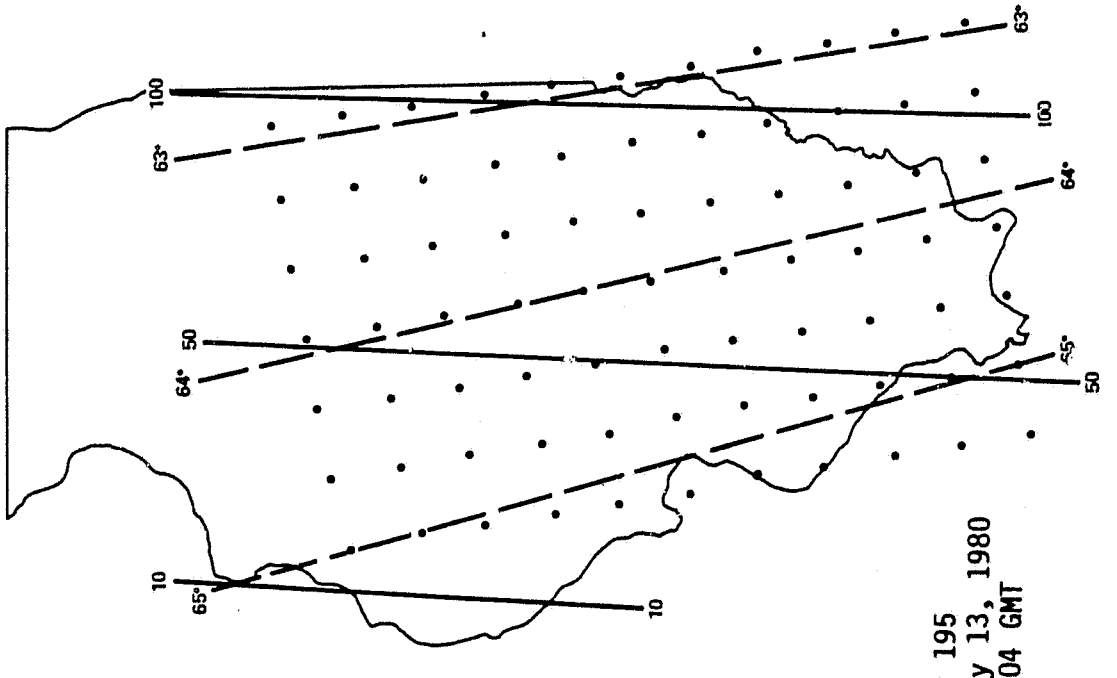

Figure D-1.- Continued.

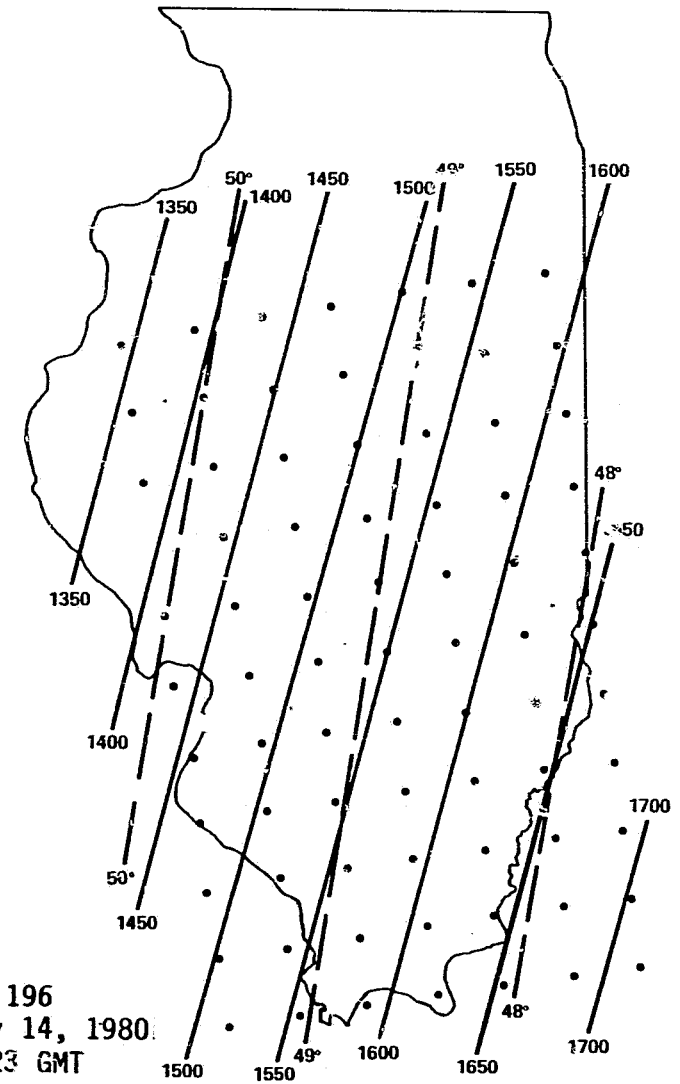

Day 196
July 14, 1980
14:23 GMT

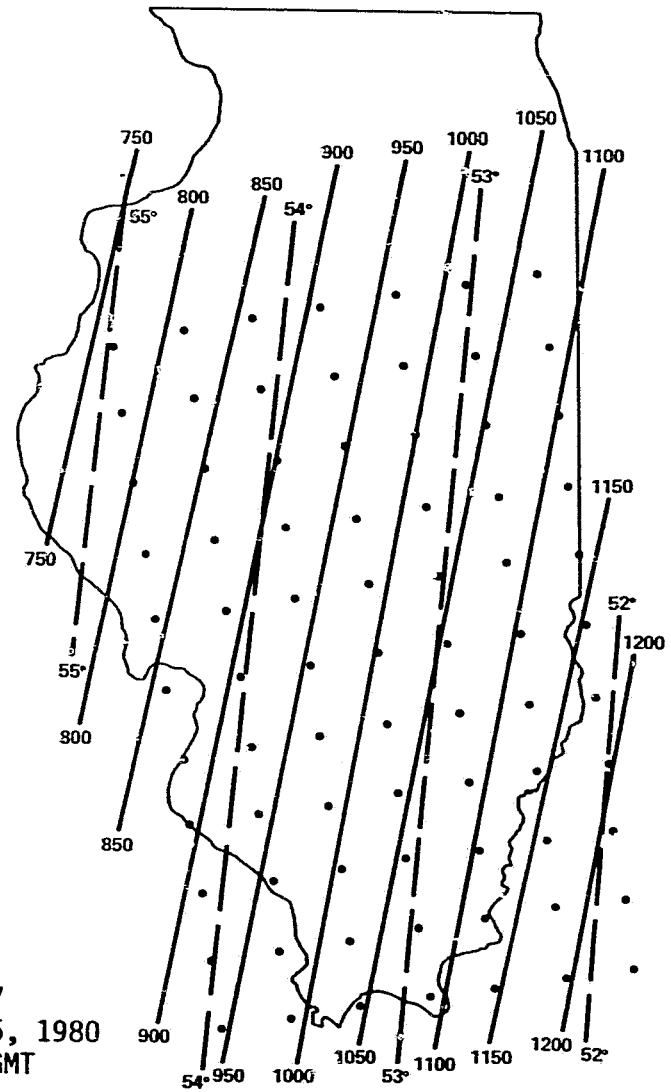

Day 197
July 15, 1980
14:01 GMT

Figure D-1.- Continued.

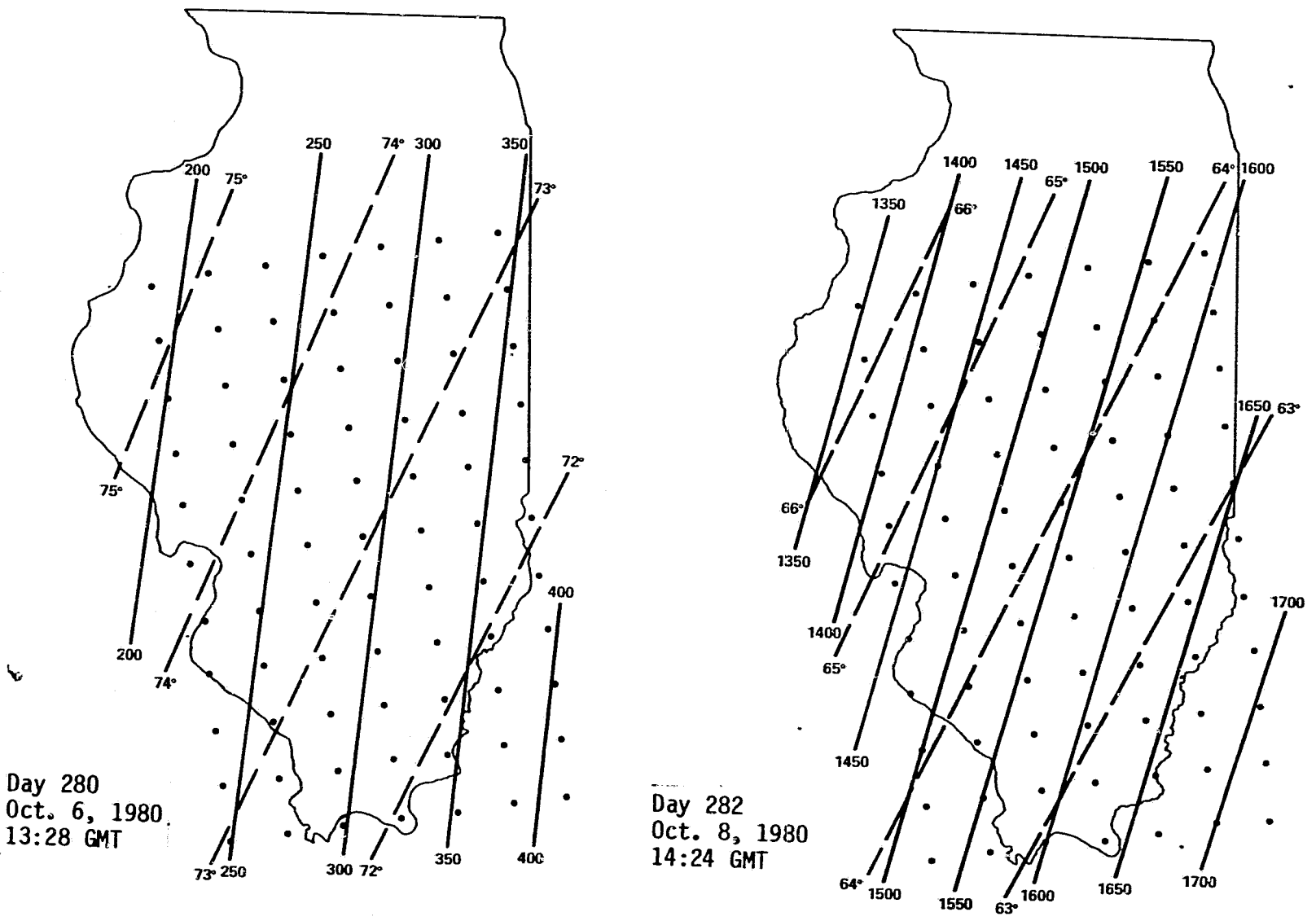

Figure D-1.- Continued.

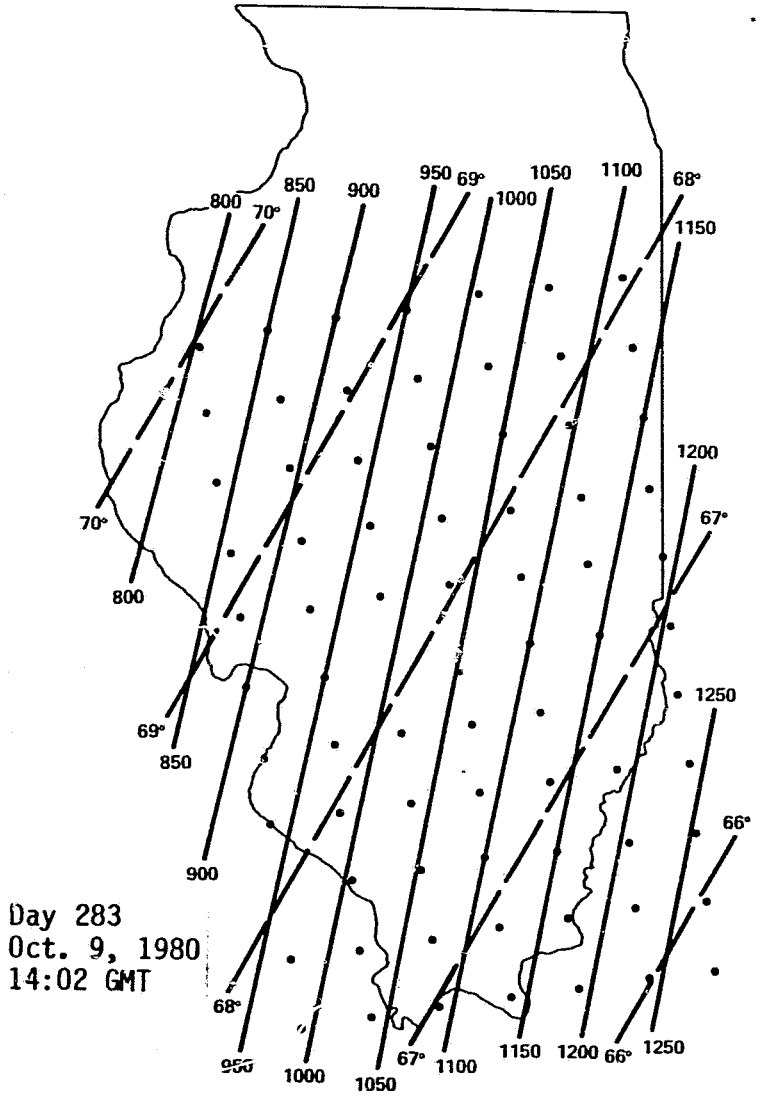

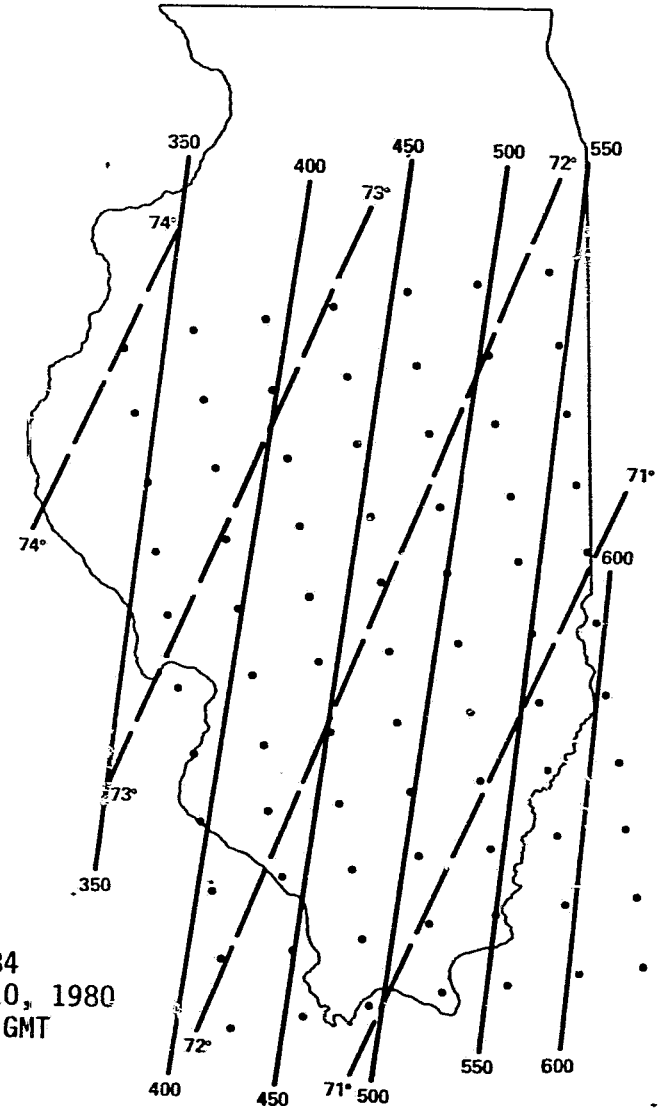

Figure D-1.- Concluded.

APPENDIX E

SATELLITE ZENITH/NADIR ANGLES VERSUS PIXEL NUMBER

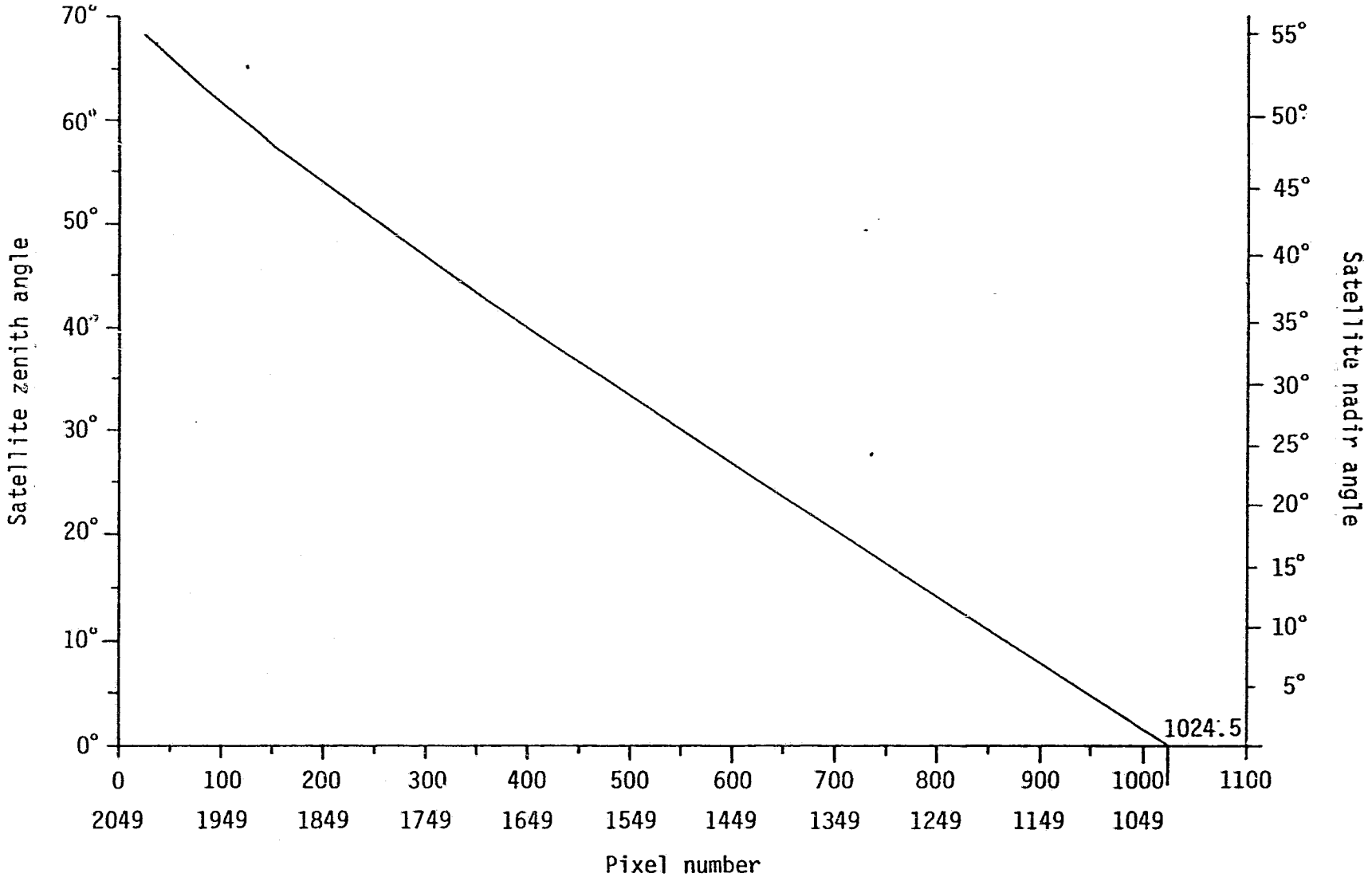

Figure E-1.- Comparison of satellite zenith angles and nadir angles with pixel numbers.

NASA-JSC